Swarthmore College
Works

Senior Theses, Projects, and Awards | Student Scholarship

2023

Synthesis and Kinetic Investigation of Oxidation in A Palladium-Methyl System

Richard A. Cardrino , '23

Follow this and additional works at: https://works.swarthmore.edu/theses

Part of the Chemistry Commons

Recommended Citation

Cardrino, Richard A. , '23, "Synthesis and Kinetic Investigation of Oxidation in A Palladium-Methyl System" (2023). *Senior Theses, Projects, and Awards*. 261.
https://works.swarthmore.edu/theses/261

This work is licensed under a Creative Commons Attribution-NonCommercial-No Derivative Works 4.0 International License.
Please note: the theses in this collection are undergraduate senior theses completed by senior undergraduate students who have received a bachelor's degree.
This work is brought to you for free by Swarthmore College Libraries' Works. It has been accepted for inclusion in Senior Theses, Projects, and Awards by an authorized administrator of Works. For more information, please contact myworks@swarthmore.edu.

SYNTHESIS AND KINETIC INVESTIGATION OF OXIDAITON IN A PALLADIUM-METHYL SYSTEM

Richard Anthony Cardrino
Senior Thesis
in
Chemistry
Presented to the Faculties of Swarthmore College
In Partial Fulfillment of the Requirements for the
Degree of Bachelor of Arts in Chemistry
2023
Advised by
Christopher R. Graves

Acknowledgments

I would like to start by acknowledging the immense amount of guidance and mentoring graciously provided by Chris Graves. From the beginning interviewing a tired young chemist via Zoom due to quarantine, Chris has been extraordinary supportive in believing in my capacity as a chemist. This collaborative research project between Swarthmore College and the University of Pennsylvania was made possible thanks to him and allowed me to explore and fall in love with the city of Philadelphia. I will always miss having mango smoothies with Chris.

Additionally, Karen Goldberg has supported me tremendously from integrating to the social life of the city of Philadelphia to making time to mentor me and guide my research project collaborating with her laboratory. She has similarly believed in my laboratory capabilities, vouching for my skills, and supporting my motion to be able to utilize the NMR facilities at the University of Pennsylvania as an undergraduate researcher.

I would like to thank all the members of the Goldberg Group for their constant advice and actively including me in the laboratory culture regardless of the amount of time that I spent on the train to commute, it was time well spent to be able to connect with these multifaceted and kind chemists. I am especially thankful for the guidance and support of Nathanael Hirscher who I am certain has gone on to make a wonderful, supportive professor.

During my undergraduate research in the Graves Group, I am thankful for having worked along many great friends and fellow chemists—Julia LeBlanc, Omar Saleh, and Joe Scott. I am grateful for the comradery that we have cultivated in the Graves Lab together supporting each other and the lifetime friendship we have developed together.

I would also like to thank my friends with a notable mention to the following: Eduardo Aguilar, Molly Erdman, Leila Kirton, Kiran McDonald, Jorge Lopez-Nava, and Devika Subedi. I am truly indebted to these wonderful people that have supported me throughout all my undergraduate experience and have distracted me away from problem sets to form memorable experiences. I look forward to future adventures.

Of course, I am thankful for my family and my cat for their constant love and support.

Abstract

The current industrial syngas process for transforming methane to methanol is an indirect process that requires the initial oxidation of methane to carbon monoxide with a subsequent reduction to form methanol under high pressure and temperature conditions. An alternative green chemical process is desirable, especially one that directly oxidizes gaseous methane to liquid methanol under mild conditions with an environmentally benign oxidant, such as dioxygen. The current study investigates the synthesis of a novel palladium complex with activated methane and the selective oxidation of this complex resulting in the liberation of methanol under more ambient conditions, a model system for the intermediate oxidation and functionalization steps of selective conversion of methane to methanol. A kinetic investigation was carried out to elucidate a mechanism for the selective oxidation culminating in a kinetic rate law and a proposed radical mediated reaction mechanism.

List of Common Abbreviations

$(CD_3)_2CO$ = acetone-d_6

CD_3CN = acetonitrile-d_3

AIBN = 2,2′-Azobis(2-methylpropionitrile)

C_6D_6 = benzene-d_6

bipy = 2,2′-bipyridine

BPI = 1,3-bis(2-(4-*tert*-butyl)pyridylimino)isoindole

$CHCl_3$ = chloroform

$CDCl_3$ = chloroform-d_1

DCM = dichloromethane

DOSY = Diffusion ordered spectroscopy

EtOAc = ethyl acetate

Et_2O = ethyl ether

*m*CPBA = *meta*-chloroperoxybenzoic acid

Me = methyl

TMEDA = N,N,N′,N′-Tetramethylethylenediamine

TsCl = 4-Toluenesulfonyl chloride

TEA = triethylamine

Mes = 1,3,5-Trimethylbenzene

NTf_2 = triflimide

TFA = trifluoracetic acid

(VT-)NMR = (varied temperature) nuclear magnetic resonance

Table of Contents

Acknowledgments iii

Abstract iv

List of Figures viii

List of Schemes ix

List of Tables x

1. Introduction 1

1.1 Natural Gas and Industrial Transformation *1*

1.2 Selective Oxidation of Methane *3*

1.3 Proposed Synthetic and Mechanistic Investigation *8*

2. Results & Discussion 11

2.1 Synthesis *11*
2.1.1 Organic Ligand Framework 11
2.1.2 Inorganic Framework 14
2.1.3 Preparation of **1** [(BPI)Pd(Me)] 15
2.1.4 Preparation of **2** [^{H}(BPI)Pd(Me)][BF_4] 15

2.2 Kinetic Investigation *17*
2.2.1 Aromatic Region throughout Oxidation Reaction 18
2.2.2 Small Carbon Products Formed 21
2.2.3 Kinetic Rate Law 26
2.2.4 Proposed Mechanism 31

3. Conclusion & Future Directions 35

4. Materials and Methods 37

4.1 Physical Measurements *37*

4.2 Synthetic and Characteristic Protocol *37*

4.3 Organic BPI Framework *38*
4.3.1 Synthesis of 4-(tert-butyl)pyridine-N-oxide 38
4.3.2 Synthesis of 2-amino-4-(tert-butyl)pyridine 39
4.3.3 Synthesis of 1,3-bis(2-(4-tert-butyl)pyridylimino)isoindole (BPI) 41

4.4 Inorganic Pd Framework *42*
4.4.1 Synthesis of [(TMEDA)Pd(Cl_2)] 42
4.4.2 Synthesis of [(TMEDA)Pd(Me_2)] 43

4.5 Preparation of Pd catalyst *44*
4.5.1 Synthesis of [(BPI)Pd(Me)] 44
4.5.2 Synthesis of [^{H}(BPI)Pd(Me)][BF_4] 45

4.6 DOSY *46*

4.7 Kinetics *47*
4.7.1 Rate Determination Kinetics 47
4.7.2 Spike Experiments 48

5. References 49

6. Supplementary Information 52

List of Supplementary Figures *54*

List of Figures

Figure 1. Total energy supply for the world in terajoules (TJ) based on energy source for 1990-2019. Figure borrowed from IEA **2**
Figure 2. Symmetric resolution of aromatic region of the ^{1}H NMR spectrum consistent with the symmetric resolution of the aromatic backbone of **2** going to **3** **19**
Figure 3. 2D DOSY NMR (400MHz; CD_3CN) for complex **2** **21**
Figure 4. Partial ^{1}H NMR spectra showing the prodcution of methanol and methyl hydroperoxide **22**
Figure 5. Spike experiment validating formation of methanol **24**
Figure 6. Spike experiment validating formation of formaldehyde **25**
Figure 7. Zero order dependence on O_2 ..... **27**
Figure 8. ½ order dependence on **2** **28**
Figure 9. Alternative fittings for dependence on **2** **29**
Figure 10. ½ order dependence on AIBN **30**
Figure 11. 1st order fitting for AIBN **31**

List of Schemes

Scheme 1. Conversion of methane to methanol via the industrial syngas method 3
Scheme 2. R–H bond activation methods to activate the C–H bond of methane 4
Scheme 3. Proposed general catalytic cycle for the selective oxidation of methane to methanol. 5
Scheme 4. Arene C–H activation of C_6H_6 with [^{H}(BPI)Pt(Me)][NTf_2] 6
Scheme 5. Oxidation of [(bipy)Pd(Me)$_2$] to [(bipy)Pd(Me)(OOMe)] utilizing elemental dioxygen 7
Scheme 6. Proposed mechanism for the oxidation of [(bipy)Pd(Me)$_2$] to [(bipy)Pd(Me)(OOMe)] utilizing O_2 and the temperature sensitive radical initiator AIBN 8
Scheme 7. Left to right complexes **1** [(BPI)Pd(Me)]; **2** [^{H}(BPI)Pd(Me)][BF_4]; 3 [(BPI)Pd(CD_3CN)][BF_4] 9
Scheme 8. Standard synthesis of 4-(*tert*-butyl)pyridine-*N*-oxide 11
Scheme 9. Adapted synthesis of 2-amino-4-(*tert*-butyl) 12
Scheme 10. Modified synthesis for BPI 13
Scheme 11. Standard synthesis of [(TMEDA)Pd(Cl)$_2$] 14
Scheme 12. Standard synthesis of [(TMEDA)Pd(Me)$_2$] 15
Scheme 13. Synthesis of [(BPI)Pd(Me)] 15
Scheme 14. Improved synthesis of [^{H}(BPI)Pd(Me)][BF_4] 17
Scheme 15. Proposed reaction of **2** with AIBN and O_2 at 60°C in CD_3CN producing **3** and MeOH. 18
Scheme 16. Reaction of **2** with O_2 in the presence of AIBN to be kinetically investigated to experimentally derive a kinetic rate law 26
Scheme 17. Proposed mechanism for the reaction of **2** with O_2 utilizing AIBN to form the oxidation product [^{H}(BPI)Pd(OOMe)][BF_4] 32
Scheme 18. Synthetic scheme for 4-(*tert*-butyl)pyridine-*N*-oxide 38
Scheme 19. Synthetic scheme for 2-amino-4-(*tert*-butyl)pyridine. 39
Scheme 20. Synthetic scheme for BPI 41
Scheme 21. Synthetic scheme for [(TMEDA)Pd(Cl)$_2$] 42
Scheme 22. Synthetic scheme for [(TMEDA)Pd(Me)$_2$] 43
Scheme 23. Synthetic scheme for [(BPI)Pd(Me)] 44
Scheme 24. Synthetic scheme for [^{H}(BPI)Pd(Me)][BF_4] 45

List of Tables

Table 1. The acquisition parameters for DOSY of [^{H}(BPI)Pd(Me)][BF_4]**.....46**

1. Introduction

1.1 Natural Gas and Industrial Transformation

Natural gas, primarily composed of methane, is an important energy source and is increasing in use as global energy consumption shifts from a dependance on oil towards other carbon based sources (**Figure 1**).[1] Unfortunately methane is expensive to transport due to its volatile gaseous state under standard conditions;[2] oil fields, locations enriched in natural gas, transform the methane into CO_2 through the flaring process. This flaring process which combusts the natural gas is carried out as the release of methane into the environment has more environmental ramifications than CO_2, being a more potent greenhouse gas than CO_2 by 84 fold on a 20-year scale.[3] Alternatively, converting the methane in natural gas to methanol—a liquid under standard conditions which can be more easily transported—presents itself as a valuable, cheaper option to utilize this significant fuel source.[2,4]

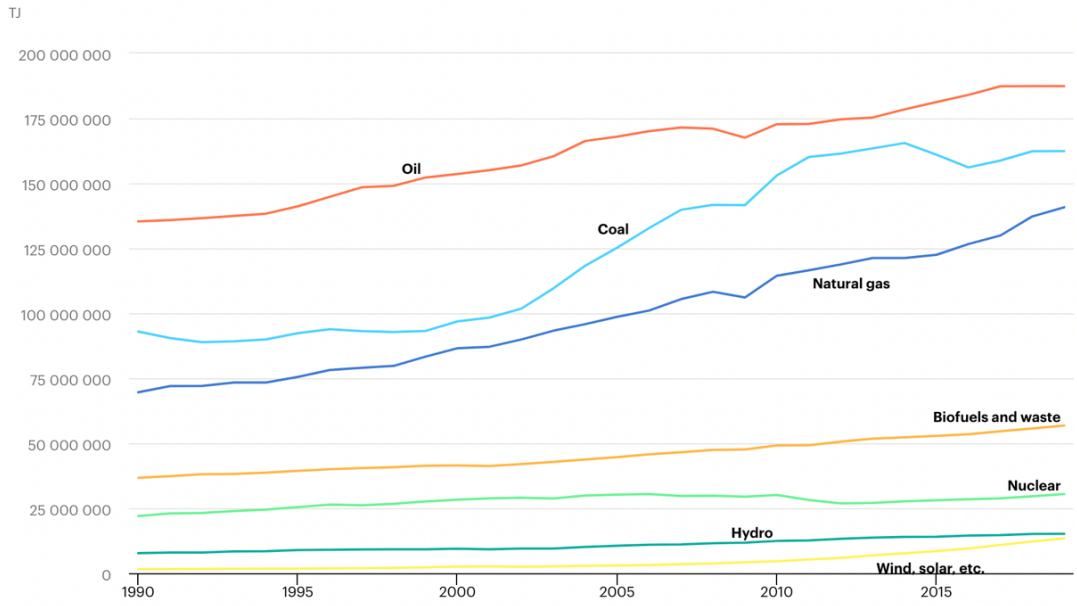

Figure 1. Total energy supply for the world in terajoules (TJ) based on energy source for 1990-2019. Figure from IEA.[1]

Methanol is also a significant chemical precursor applicable in many synthetic chemical industries as a solvent or small carbon source for conversion into olefins as well as gasoline.[4] Currently, the syngas method is the only industrially used process to convert methane to methanol.[2] This energy intensive process includes an oxidative step at high temperatures (1173 K) and pressures (100 bar) to break all C–H bonds in methane, forming syngas—a gaseous mixture of CO and H_2. A secondary reductive step is then required to reduce carbon monoxide to finally form methanol (**Scheme 1**).[2,5]

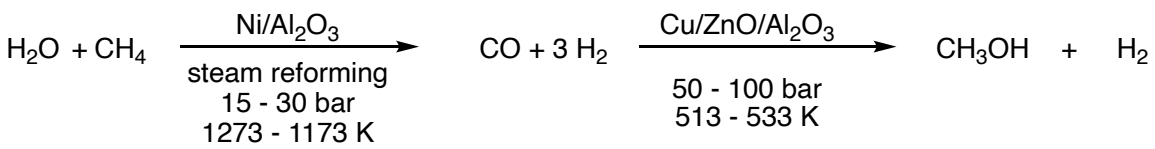

Scheme 1. Conversion of methane to methanol via the industrial syngas method.

This indirect conversion of methane to methanol is inefficient and costly. More efficient selective oxidation of methane under mild conditions is a process of interest to be able to productively utilize this limited resource.

1.2 Selective Oxidation of Methane

Development of a catalyst capable of selectively oxidizing methane to methanol under mild conditions would have a significant impact on methanol production. It would also embrace the movement towards green chemistry, a field of chemistry focused on improved sustainability and safety.[6]

Functionalization of alkanes, especially methane, into higher order chemicals and fuels is an active area of research.[3] A common hurdle and first step in functionalizing alkanes is C–H bond activation. Common mechanisms for C–H bond activation include oxidative addition (OA), concerted metalation deprotonation (CMD), and metal-ligand cooperation (MLC) (**Scheme 2**).[8] MLC and CMD are of particular interest. In both instances the oxidation state of the metal ion of a potential catalyst is conserved. MLC is particularly attractive due to the concerted localization of the proton in the coordination sphere unlike CMD.

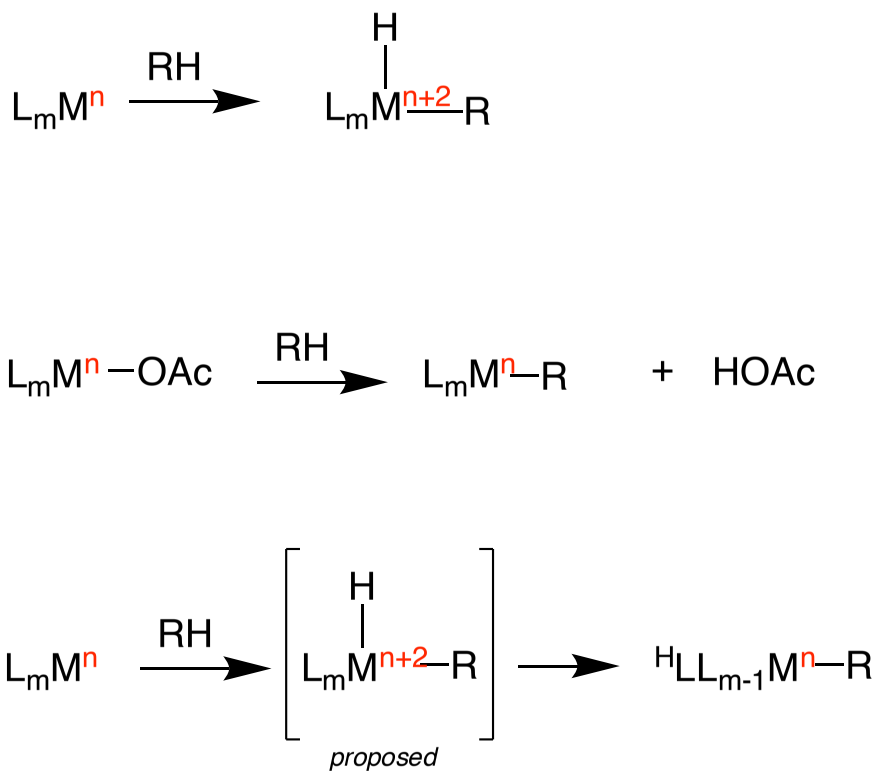

Scheme 2. R–H bond activation methods to activate the C–H bond of methane.

This conservation of metal oxidation state is important as this is conducive to desirable reactivity under aerobic conditions. This allows for exploitation of the tendency of metal complexes to oxidative in the presence of air, utilizing O_2 in the atmosphere as an environmentally benign and abundant oxidant, to produce productive oxidative products. Interestingly, the oxidation mechanisms of organometallic complexes with O_2 are still poorly understood.

This thesis work aims to investigate novel palladium-based catalysts that can oxidize methane to methanol to fill this void to better understand the mechanisms of this catalytic selective oxidation. To oxidize methane to methanol, a catalytic cycle can be imagined in which the C–H bond is activated, followed by the oxidation of the activated alkane, and further functionalization to liberate free methanol (**Scheme 3**).

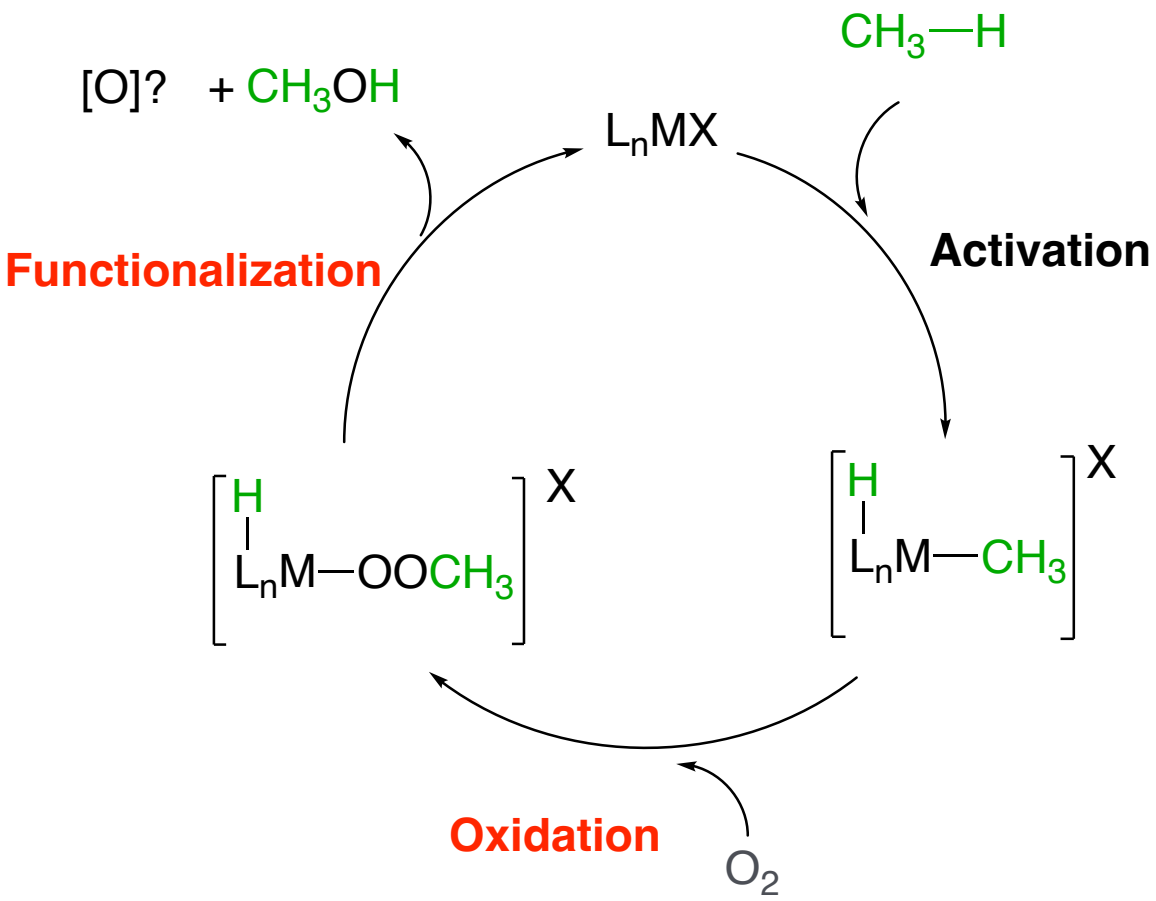

Scheme 3. Proposed general catalytic cycle for the selective oxidation of methane to methanol. The red processes of oxidation and functionalization will be investigated in this study. The fate of the supplementary oxygen atom resulting from the functionalization step is unknown.

The Goldberg group has investigated the use of palladium and platinum based complexes that are capable of activating the C–H bond in methane as well as oxidizing to form the metal-methyl peroxide species (**Scheme 3**)[8-9]. Previous work investigated the use of a platinum based complex capable of activating the C–H bond such as those found in arenes such as benzene (**Scheme 4**).[8]

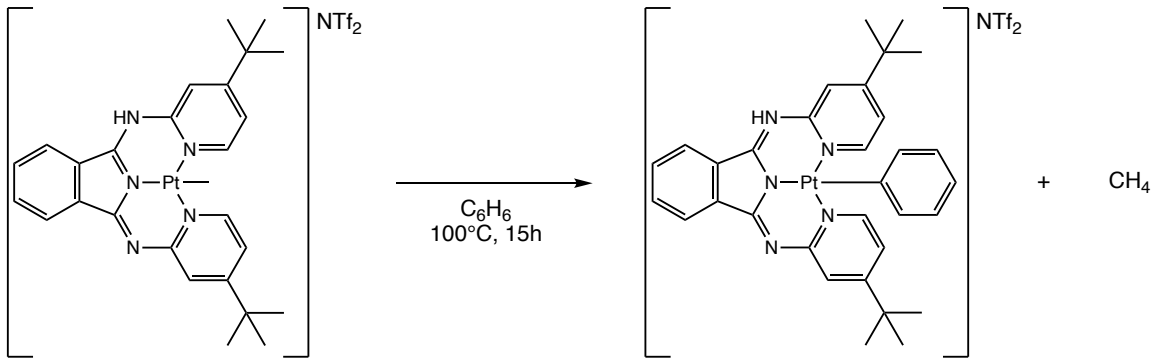

Scheme 4. Arene C–H activation of C_6H_6 with [^{H}(BPI)Pt(Me)][NTf_2].

Zeitler et al. demonstrated that [^{H}(BPI)Pt(Me)][NTf_2] (BPI = 1,3-bis(2-(4-*tert*-butyl)pyridylimino)isoindole); NTf_2 = triflimide) was capable of activating the C–H bond found in benzene. These results also demonstrated the importance of the counter-ion in metal-ligand-anion cooperative (MLAC) reaction. In MLAC reactions, the metal oxidation state is conserved as well as the localization of a proton in the coordination sphere with an additional benefit of a cooperative counterion that could contribute to functionalization of the proton in subsequent reactions.[8] This localized ion could act as a shuttle for the proton on the organic ligand framework to facilitate transportation of the proton from the ligand framework to form the alcohol hydrogen in the final functionalized MeOH product. A few groups have also studied the use of elemental dioxygen as an oxidant for the selective oxidation of methane in the presence of organometallic catalysts, though not all cases result in the production of free oxidized methyl derivatives.[8,10–13]

Additional work by the Goldberg and Britovsek groups focused on the oxidation of metal-methyl complexes utilizing elemental dioxygen.[8,12-13] In successful instances of oxidation, the resulting product was a metal-methyl peroxide species. The Britovsek group studied this oxidation catalyzed by light whereas the Goldberg group utilized a

temperature sensitive radical initiator AIBN (AIBN = 2,2′-Azobis(2-methylpropionitrile)) to probe the kinetics of the oxidation in a controlled manner to elucidate a mechanism for oxidation.[8,12-13]

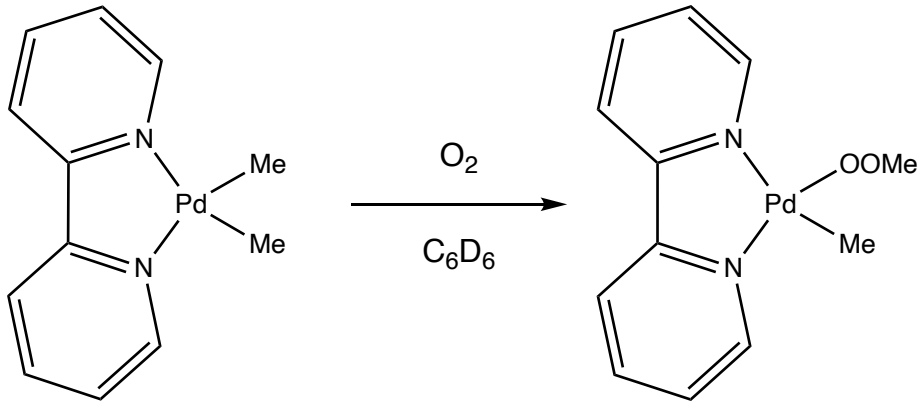

Scheme 5. Oxidation of [(bipy)Pd(Me)$_2$] to [(bipy)Pd(Me)(OOMe)] utilizing elemental dioxygen.

The oxidation of activated methane in [(bipy)Pd(Me)$_2$] (bipy = 2,2′-bipyridine) to the methyl peroxide species in [(bipy)Pd(Me)(OOMe)] (**Scheme 5**) was studied and a radical mediated mechanism was proposed for this selective oxidation (**Scheme 6**).[9] Late transition metals such as palladium are of particular interest in developing a catalytic cycle as they are well documented to accomplish the initial step of activating the C–H bond such as that found in methane.[15] Observing this oxygen insertion provides the possibility of developing a palladium oxygenase catalyst that is capable of activating the C–H bond, followed by the insertion of oxygen, and a further functionalization step to regenerate the palladium catalyst and liberate oxidized alkanes.[14-15] This preliminary mechanism observed by Boisvert et al. for the oxidation of a Pd–Me complex to form the Pd–OOMe species is promising for future development of a catalyst that may further functionalize this peroxy-species, forming free methanol.[9] The recently proposed mechanism is consistent with the experimental rate law of one-half order with respect to

both AIBN and [(bipy)Pd(Me)$_2$] which diverges from previous oxidation mechanism such as O_2 insertion into Pd–H which do not follow a radical chain mechanism (**Scheme 6**).[9,11,17]

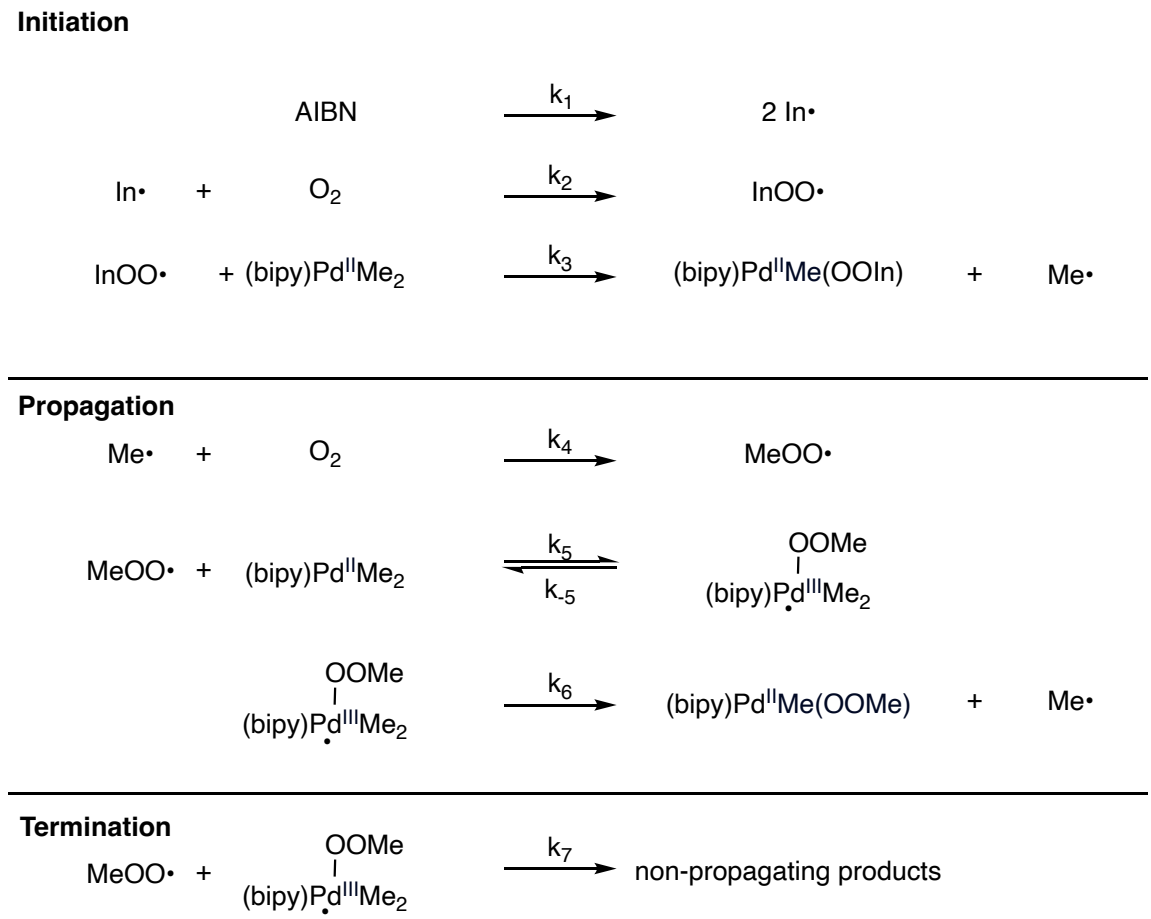

Scheme 6. Proposed mechanism for the oxidation of [(bipy)Pd(Me)$_2$] to [(bipy)Pd(Me)(OOMe)] utilizing O_2 and the temperature sensitive radical initiator AIBN.

1.3 Proposed Synthetic and Mechanistic Investigation

In this proposed work, the novel complex **2** [^{H}(BPI)Pd(Me)][BF_4] (**Scheme 7**) was synthesized and characterized. Once prepared, a mechanistic investigation was carried out to study the selective oxidation of Pd–Me to MeOH with elemental dioxygen

utilizing this complex. A radical mediated mechanism with dioxygen insertion similar to previous work by the Goldberg group was expected in this Pd system.[10]

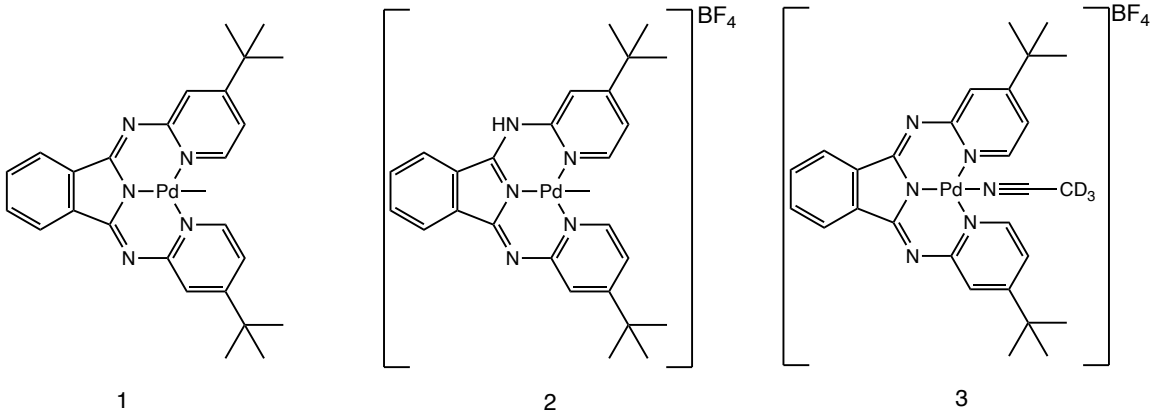

Scheme 7. Left to right complexes **1** [(BPI)Pd(Me)]; **2** [^{H}(BPI)Pd(Me)][BF_4]; **3** [(BPI)Pd(CD_3CN)][BF_4].

1 [(BPI)Pd(Me)] (**Scheme 7**) was prepared using a Methyl-then-Ligand approach, synthesizing the organic BPI framework and an inorganic methylated palladium species separately before introducing the organic BPI ligand framework to the palladium complex. The synthesis of the organic ligand as well as the inorganic synthetic procedures of preparing the catalysts were optimized. **1** was then be protonated to form the principal complex of interest **2** [^{H}(BPI)Pd(Me)][BF_4] (**Scheme 7**) which was then characterized utilizing nuclear magnetic resonance (NMR) spectroscopy.

The kinetic investigation probed the oxidation and functionalization steps of the proposed catalytic cycle in this system (**Scheme 3)**. **2** was reacted with elemental dioxygen in the presence of the temperature dependent radical initiator—AIBN—to form the acetonitrile derivative **3** [(BPI)Pd(CD_3CN)][BF_4] (**Scheme 7**). The temperature dependent radical initiator allowed the suspected radical mediated reaction to occur in a controlled manner and the reaction was studied by variable temperature nuclear magnetic

resonance spectroscopy (VT-NMR). The presence of a nonreactive internal standard—mesitylene (Mes)—allowed for quantification of the reaction using the integrals of the NMR signals to track product formation over time. A kinetic rate law for this selective oxidation and functionalization of Pd–Me to MeOH was discovered and a mechanism was proposed.

2. Results & Discussion

2.1 Synthesis

2.1.1 Organic Ligand Framework

Preparation of 4-(*tert*-butyl)pyridine-*N*-oxide followed standard literature procedures (**Scheme 8**) and yielded a yellow solid (99% yield) (**Figure S1**).[18]

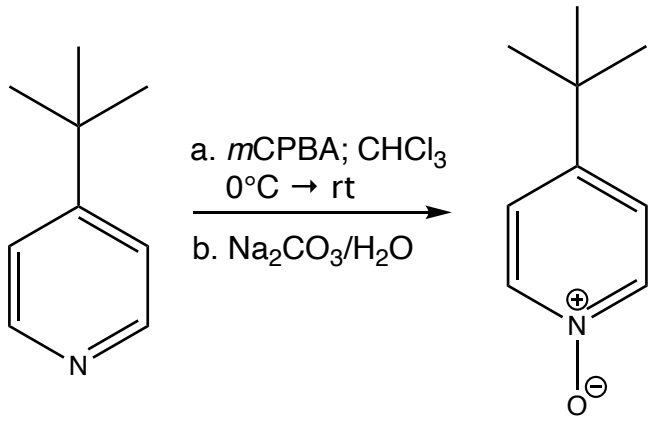

Scheme 8. Standard synthesis of 4-(*tert*-butyl)pyridine-*N*-oxide.

Preparation of 2-amino-4-(*tert*-butyl)pyridine was modeled after standard literature procedures (**Scheme 9**).[18] 4-(*tert*-butyl)pyridine-*N*-oxide was allowed to react with (*tert*-butyl)amine in DCM. 4-Toluenesulfonyl chloride (TsCl) was slowly added and allowed to react stirring overnight. The reaction was observed to be incomplete which diverged from traditional literature results; thus, the reaction was recharged with TsCl. Incomplete conversion observed by ^{1}H NMR spectroscopy was still observed; therefore, (*tert*-butyl)amine and TsCl were recharged into the reaction and allowed to stir overnight. Incomplete conversion persisted as noted by ^{1}H NMR spectroscopy; therefore, more (*tert*-butyl)amine was added along with a slow addition of TsCl and the reaction, after

complete conversion was observed, was worked up with an aqueous NaOH solution. The product was extracted with DCM and dried with $MgSO_4$ and *in vacuo*.

The products of this initial step underwent a preliminary purification to remove side products that formed from the reaction of (*tert*-butyl)amine with TsCl. This preliminary purification would allow for the use of less trifluoracetic acid (TFA) in the deprotection step of the amination, rendering this step safer as compared to standard literature procedure which performed the deprotection in the crude reaction mixture.[18] A recrystallization utilizing warm EtOAc and hexanes was performed and filtrate was collected and dried *in vacuo*. Dried organics were reacted with TFA and heated to 90°C overnight. The reaction mixture was quenched with an aqueous NaOH solution and extracted with DCM and dried with $MgSO_4$ and *in vacuo*. The resulting oil was dry loaded onto a silica gel column equilibrated with 1:1 EtOAc : hexanes, eluted, and fractions containing product were dried *in vacuo*. 2-amino-4-(*tert*-butyl)pyridine was collected as a yellow solid (56% yield) (**Figure S2**).

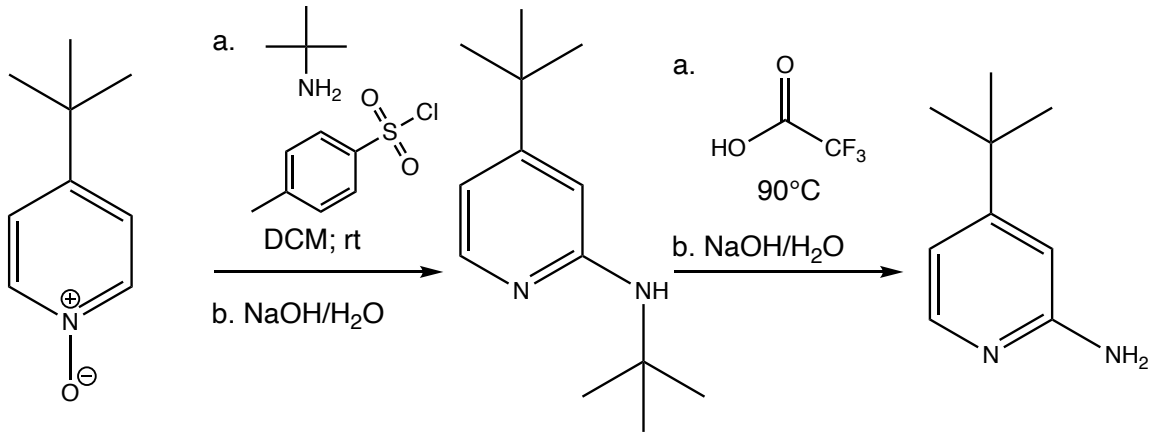

Scheme 9. Adapted synthesis of 2-amino-4-(*tert*-butyl).

The synthesis of BPI was modified from standard literature procedures due to irreproducibility of synthetic procedures (**Scheme 10**).[19] Standard literature procedures

for the synthesis of BPI resulted in excess loss of product due to solubility in hexanes during a rinsing step to remove 1-hexanol as well as impure final product.[19]

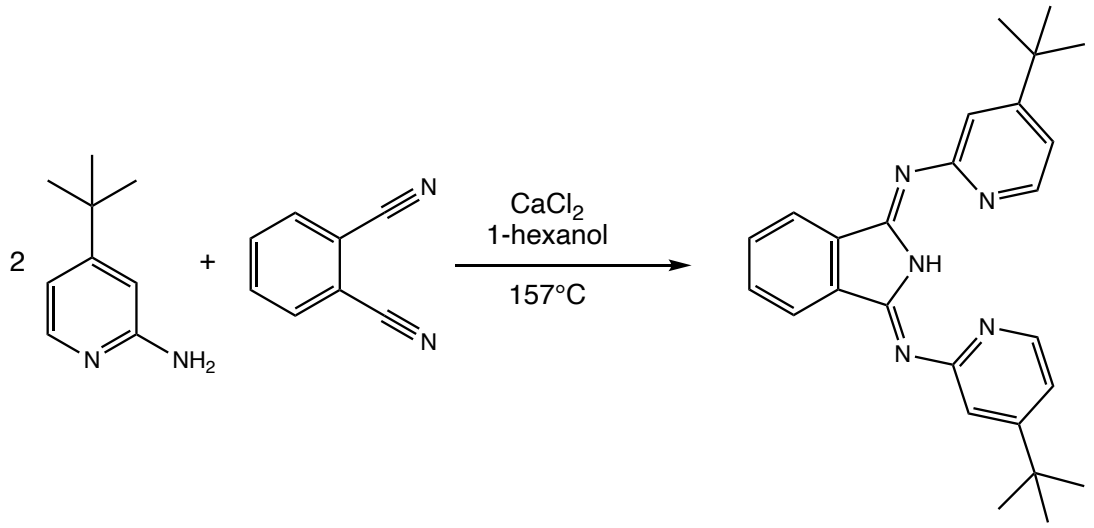

Scheme 10. Modified synthesis for BPI.

Alternatively, the resulting crude product mixture was dried *in vacuo* to remove 1-hexanol. This step allowed for successful removal of all of the 1-hexanol and resulted in more pure product as compared to syntheses that followed literature procedures.[19]

The resulting solids were transferred to a frit with H_2O due to low solubility of product in H_2O and rinsed in excess to remove calcium salts that formed during reaction. Finally, the resulting brown crude mixture was rinsed with cold hexanes to remove an unknown brown impurity while maintaining low solubility of BPI product. The implementation of cold hexanes improved yield. The yellow filtrand was then dissolved in DCM and filtered. The resulting yellow filtrate was dried *in vacuo* to yield pure BPI (**Figure S3**) with an unknown solid blue filtrand impurity remaining on the sintered glass frit. These procedures increased yield (69% yield) and purity (lack of 1-hexanol) as

compared to prior attempts of this synthesis performed by former Goldberg group members.

2.1.2 Inorganic Framework

Preparation of [(TMEDA)Pd(Cl)$_2$] (TMEDA = N,N,N′,N′-tetramethylethylenediamine) followed standard literature procedures (**Scheme 11**), yielding a yellow powder (96% yield) (**Figure S4**).[20]

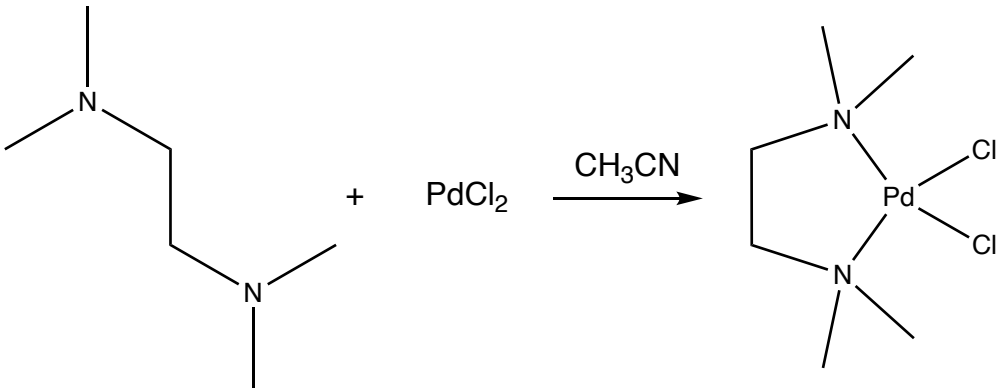

Scheme 11. Standard synthesis of [(TMEDA)Pd(Cl)$_2$].

Preparation of [(TMEDA)Pd(Me)$_2$] also followed standard literature procedures (**Scheme 12**), yielding a white solid (52% yield) (**Figure S5**).[20]

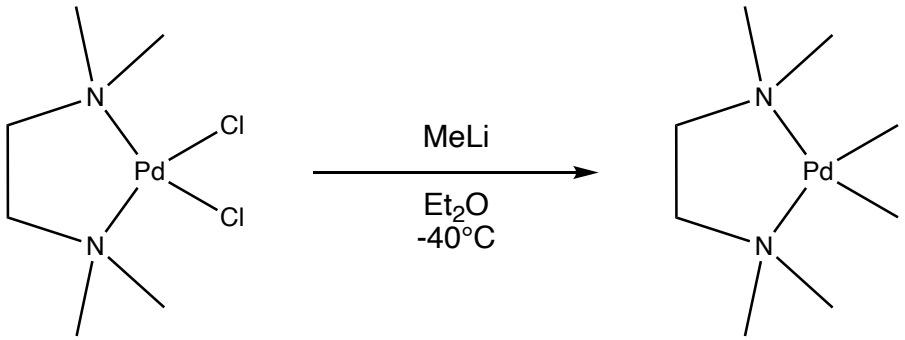

Scheme 12. Standard synthesis of [(TMEDA)Pd(Me)$_2$].

*2.1.3 Preparation of **1** [(BPI)Pd(Me)]*

BPI was reacted with [(TMEDA)Pd(Me)$_2$] in benzene overnight at 60°C (**Scheme 13**). The red solution was dried and a red powder of **1** was collected (**Figure S6**). This protocol was previously optimized by the Goldberg group and yielded consistent reactivity, purity, and yield (94% yield).

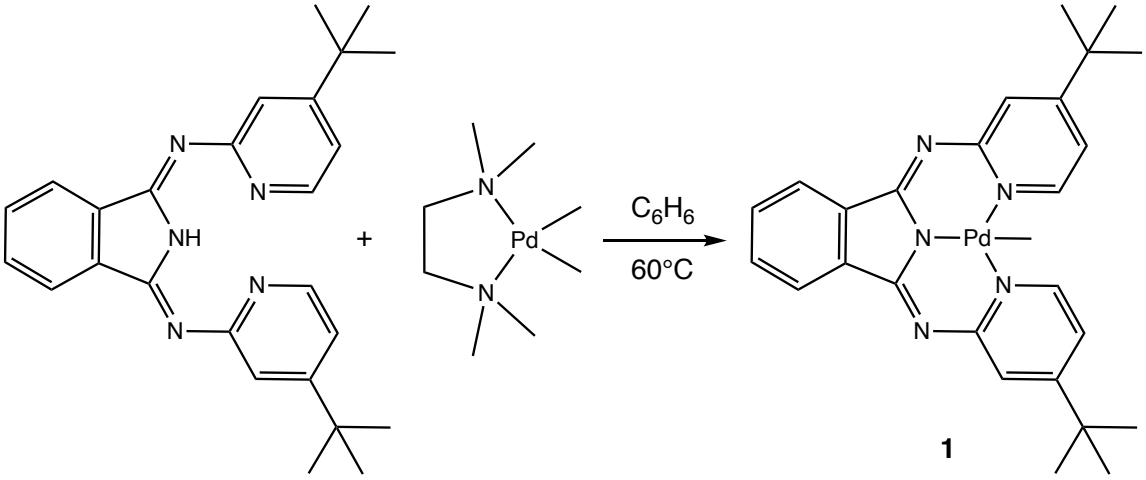

Scheme 13. Synthesis of [(BPI)Pd(Me)].

*2.1.4 Preparation of **2** [^{H}(BPI)Pd(Me)][BF$_4$]*

Synthetic improvements have been made to optimize the yield and purity of **2**. Prior synthetic protocols towards **2** involved the dissolving of **1** in Et_2O followed by

addition of the resultant solution to a flask containing one molar equivalent of HBF_4 solution (50-55% w/w in Et_2O). This resulted in the immediate precipitation of a crude product of **2** upon addition to HBF_4. A following purification step involved a slow evaporation recrystallization of **2** dissolved in DCM with an Et_2O bath, which led to a black precipitate suspected to be palladium black and low yields of product (19%). To optimize this reaction, a slower addition of a more dilute solution of HBF_4 to the solution of **1** was used to slow down the reaction and improve purity (**Scheme 14**). We thought by introducing a dilute solution of HBF_4 more slowly, this would decrease the probability of potentially doubly protonating **1**. This decreased introduction of the highly reactive superacid HBF_4 would allow for slower reactivity yielding more homogenous reactivity within the reaction flask thus increasing the purity of this reaction.

We also targeted, the potential elimination of the purification step involving DCM, a known coordinating solvent that may facilitate the degradation of **2** to palladium black, was proposed. If yielding purer product was achieved, this inefficient purification processes that greatly decreases yield could be discarded.

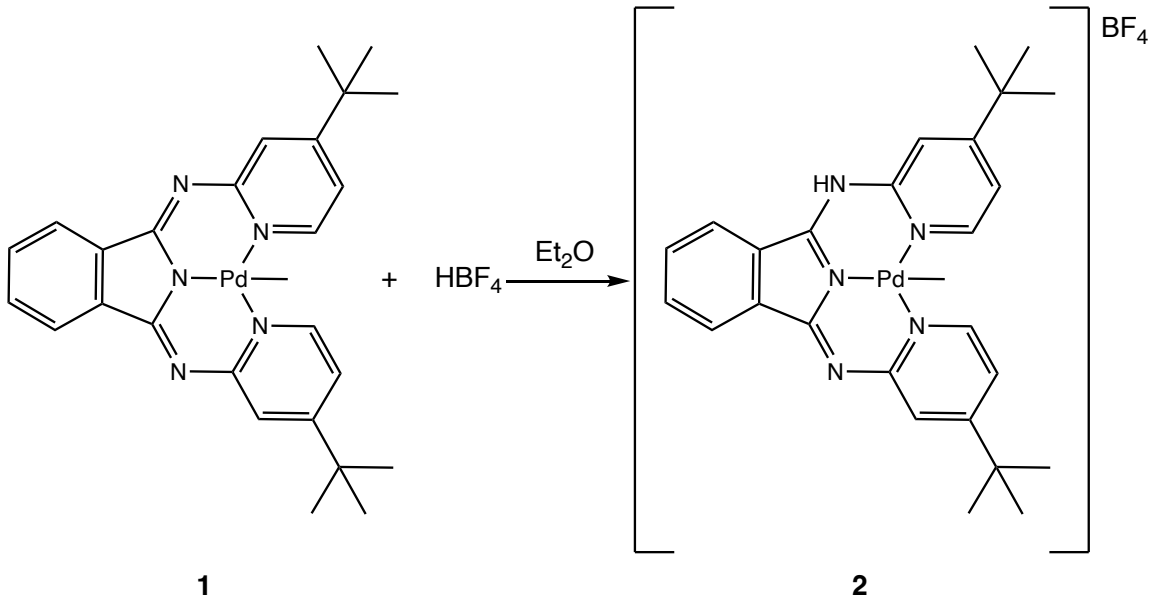

Scheme 14. Improved synthesis of [^{H}(BPI)Pd(Me)][BF_4].

As an alternative, **1** was dissolved in Et_2O. A separate fluoroboric acid solution diluted with Et_2O was prepared and slowly introduced into the reaction flask containing the solution of **1**. Upon addition of HBF_4 solution, a yellow precipitate of **2** crashed out. **2** was collected on a sintered glass frit and rinsed with Et_2O (2mL) to produce a yellow powder analyzed by ^{1}H (**Figure S7**) and ^{19}F{^{1}H} NMR spectroscopies (**Figure S8**). This product of the improved synthesis was pure and did not require a recrystallization purification step. The lack of recrystallization allowed for higher yields as pure product was formed and there was no additional degradation of product from DCM coordinating resulting in the formation of palladium black. Thus, improved yields utilizing this new method were observed (62%).

2.2 Kinetic Investigation

With **2** prepared, we next turned to the investigation into its reactivity with O_2. Prior study in the Goldberg group revealed promising selective oxidation of the Pd–Me in

2 to form liberated MeOH.[10] With this information, a kinetic investigation was of interest to begin to elucidate a reaction mechanism and compare it to prior radical mediated oxygen insertion for the Pd–Me derivative.[9–11,17] The radical initiator AIBN was utilized as it has demonstrated promising and consistent results in characterizing radical chain mediated reactivity in the Goldberg Group.[9-10] A chemical radical initiator was utilized in place of a photocatalytic initiation due to more reproducible results and resources in the Goldberg Group.[14,17] A kinetic investigation utilizing VT-NMR allowed for the experimental determination of a kinetic rate law which was then compared to prior experimental results to verify or diversify the applicability of a prior proposed radical mediated oxygen insertion into a Pd–Me bond.[9]

2.2.1 Aromatic Region throughout Oxidation Reaction

Reaction progress kinetic analysis (RPKA) was utilized to track the reactivity of **2** with elemental dioxygen as it formed **3** and produced various single carbon oxidized products, such as MeOH (**Scheme 15**).[21]

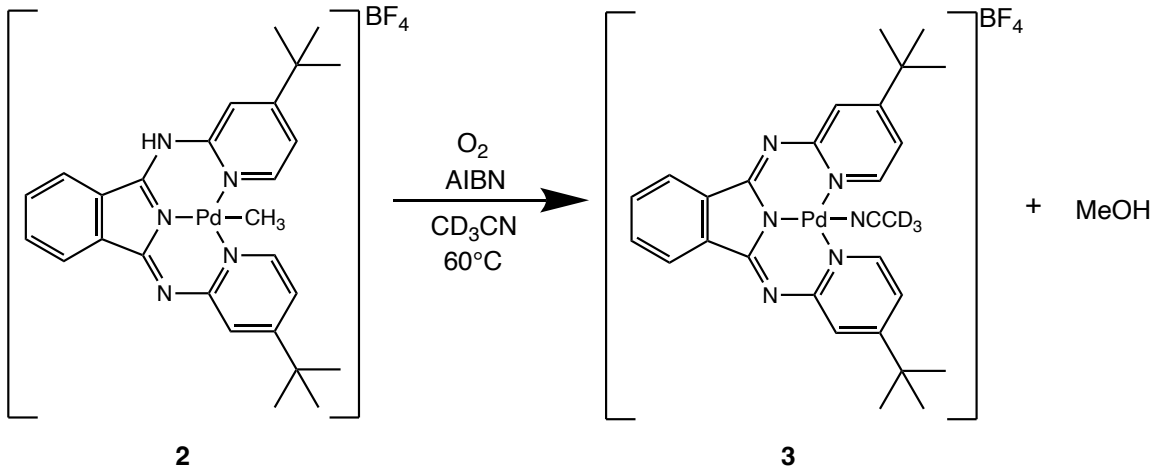

Scheme 15. Proposed reaction of **2** with AIBN and O_2 at 60°C in CD_3CN producing **3** and MeOH.

Initially, **2** presented a symmetric aromatic region as observed by ^{1}H NMR spectroscopy, despite predicted asymmetry created by the protonation of the BPI backbone (**Figure S7**). Upon pressurization with O_2, the ^{1}H NMR signals indicated an asymmetric structure followed by a symmetric resolution as product **3** was formed over time. This initially appeared to be promising to track the kinetics of the reaction of **2** with O_2 over time to give **3**; however, the processes of the aromatic region becoming asymmetric upon pressurization with O_2 is not immediate which poses a problem for obtaining reliable integrals to track reaction progress. Alternatively, the Pd–Me resonance was tracked as this had a consistent chemical shift and a reliable trackable integral to monitor reaction progress.

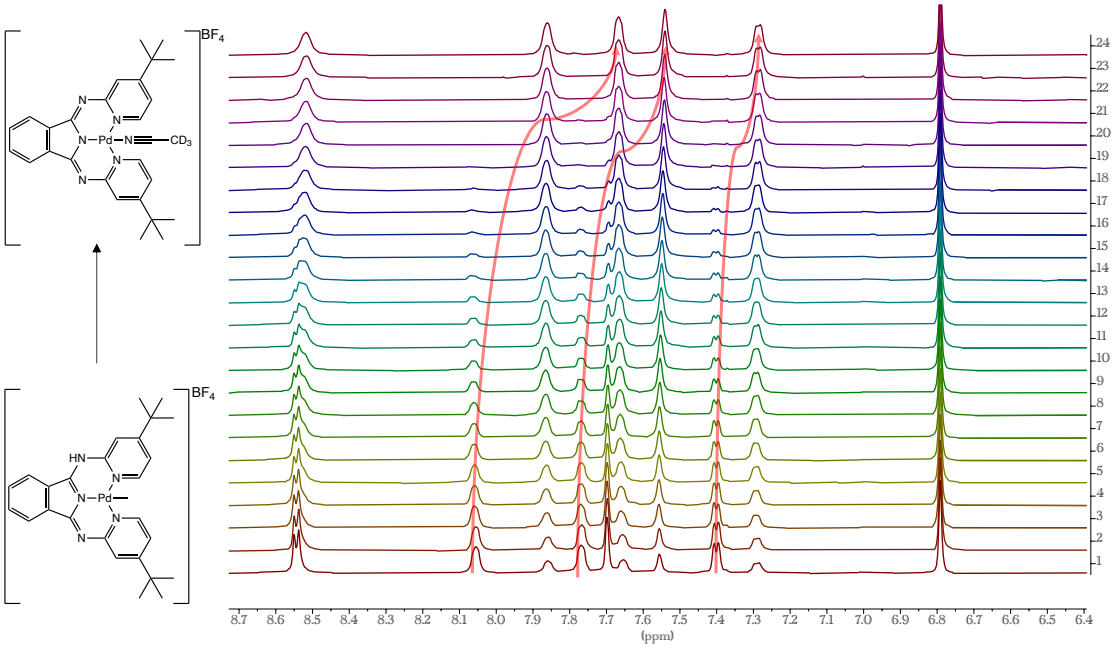

Figure 2. Symmetric resolution of aromatic region of the ^{1}H NMR spectrum consistent with the symmetric resolution of the aromatic backbone of **2** going to **3**. Spectra collected at 240s intervals with spectrum number indicated for **2** in CD_3CN at Pd–CH_3 = 8.3mM; O_2 = 5bar; AIBN = 51 mM. δ 6.8 (s 3H) is internal standard Mes.

The unexpected symmetry of the aromatic region of **2** in the absence of O_2 prompted the suspicion of a potential initial dimer state of **2** that separates into a monomer form to react with O_2. To resolve this hypothesis, diffusion ordered spectroscopy (DOSY) was implemented to estimate the molecular mass of **2** (**Figure 3**).[22]

Utilizing a Bayesian DOSY Transform (BDT) on MestReNova version 14.2.3 with a BDT resolution factor of 1.00, a single repetition, and 128 points in the diffusion dimension, the molecular mass of **2** was estimated to be 691 g/mol which is comparable to the actual 619.82 g/mol disconfirming the presence of **2** as a dimer in solution. The estimated value differs from the expected molecular mass of **2** due to DOSY being limited in its capacity to estimate the molecular mass of complexes containing particularly heavy elements such as Pd; though, this model is useful in disconfirming the hypothesis of dimer of **2**.

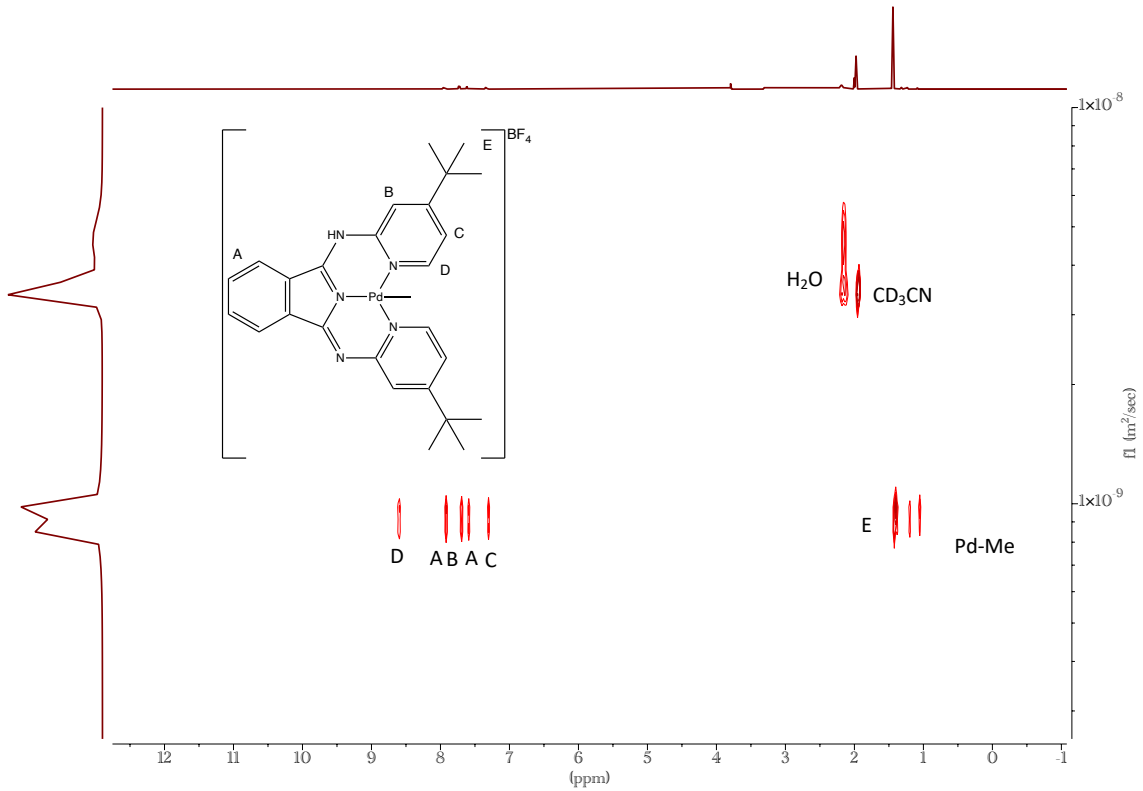

Figure 3. 2D DOSY NMR (400MHz; CD_3CN) for complex **2**. Confirmation of a monomer with estimated molecular weight of 691 g/mol.

The initial symmetry observed in the aromatic region of **2** is suspected to be due to rapid interchange of the proton position on the backbone of BPI in **2** potentially due to residual H_2O in the dried CD_3CN.

Due to the complexities of symmetry in the aromatic region, the Pd–Me resonance in the aliphatic region presented itself as a viable option to track reaction progress and thus was selected for further kinetic investigation.

2.2.2 Small Carbon Products Formed

The goal of exposing **2** to elemental dioxygen was to produce MeOH. Due to the nature of pressurizing a J Young NMR tube with O_2 to oxidize the Pd–Me in **2**, there was

concern of over oxidizing methyl to form more oxidized small carbon species. Throughout the reactivity, many small peaks grew in that were suspected to be associated with oxidized single carbon species. To confirm the identity of these species, a series of spiking experiments were performed.

The principal desired product of methanol (CH_3OH; δ 3.35) was suspected to be growing in throughout the progression of the reaction as well as methyl hydroperoxide (CH_3OOH; δ 3.81) found downfield (**Figure 4**).

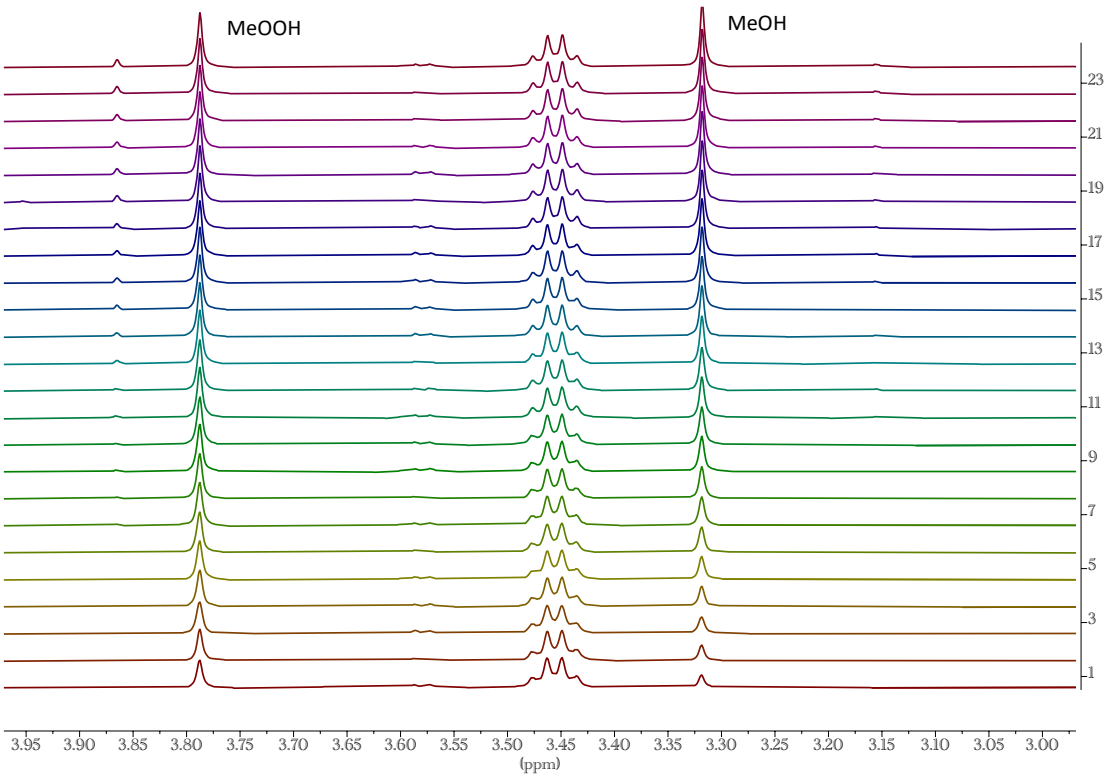

Figure 4. Partial ^{1}H NMR spectra showing the production of methanol and methyl hydroperoxide. The initial concentration of **2** = 8.3mM in CD_3CN; O_2 = 5 bar; AIBN = 51 mM with spectra collected at 240s intervals with spectrum number indicated.

The production of methanol (CH_3OH) was confirmed via a spike experiment in which the reaction J Young tube was opened to atmosphere to release the pressurized O_2 after completion of the oxidation, spiked with a small quantity of methanol (CH_3OH) (0.3

μL), and analyzed via ^{1}H NMR spectroscopy under standard atmosphere (1 bar air). This spiking confirmed the formation of methanol (CH_3OH) as the signal attributed to methanol grew larger (**Figure 5**).

There was a slight downfield shift in peaks noted in the sample that was pressured with O_2 (5 bar) and this is suspected to occur due to the presence of this paramagnetic species and was observed consistently throughout the investigation.

The presence of methyl hydroperoxide (CH_3OOH) was also suspected based on chemical shift and could have formed due to the presence of excess O_2 allowing for further oxidation of methane to methanol. Alternately, a reaction mechanism can be imagined including the insertion of oxygen into the activated methyl forming a Pd–OOMe species that releases methyl hydroperoxide (CH_3OOH) that decomposes to form the more stable methanol (CH_3OH) which is most probable and these decomposition pathways may explain the unknown fate of the extra oxygen in the functionalization step.

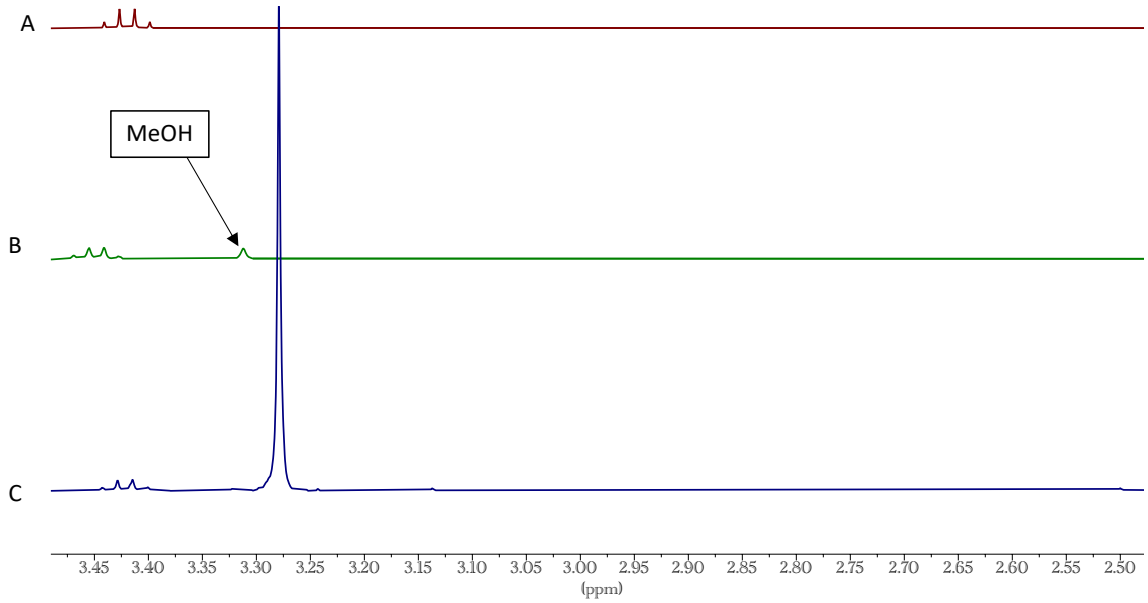

Figure 5. Spike experiment validating formation of methanol. (A) **2** Pd–CH_3 8.7 mM in CD_3CN; AIBN 52.7 mM; 298 K; t = 0 s (B) sample A pressurized with 5 bar O_2 and reaction completed; 333 K; t = 9540 s (C) sample B open to atmosphere and spiked with 0.3 µL of MeOH; 298 K. Note the change in chemical shift in spectrum C due to release of 5 bar O_2.

A similar process was carried out for the suspected formation of formaldehyde (CH_2O, δ 9.65) and peroxyformic acid (CH_2O_3, δ 9.93). After completion of the oxidation, O_2 pressure was released and a small amount of formaldehyde solution (5 µL; 37% wt formaldehyde in H_2O with 10 - 15% MeOH) was spiked in followed by further investigation with ^{1}H NMR spectroscopy. (**Figure 6**). Only the formaldehyde peak (CH_2O) grew in upon spiking confirming the formation of formaldehyde (CH_2O) throughout the progress of the oxidation reaction (**Figure 6**).

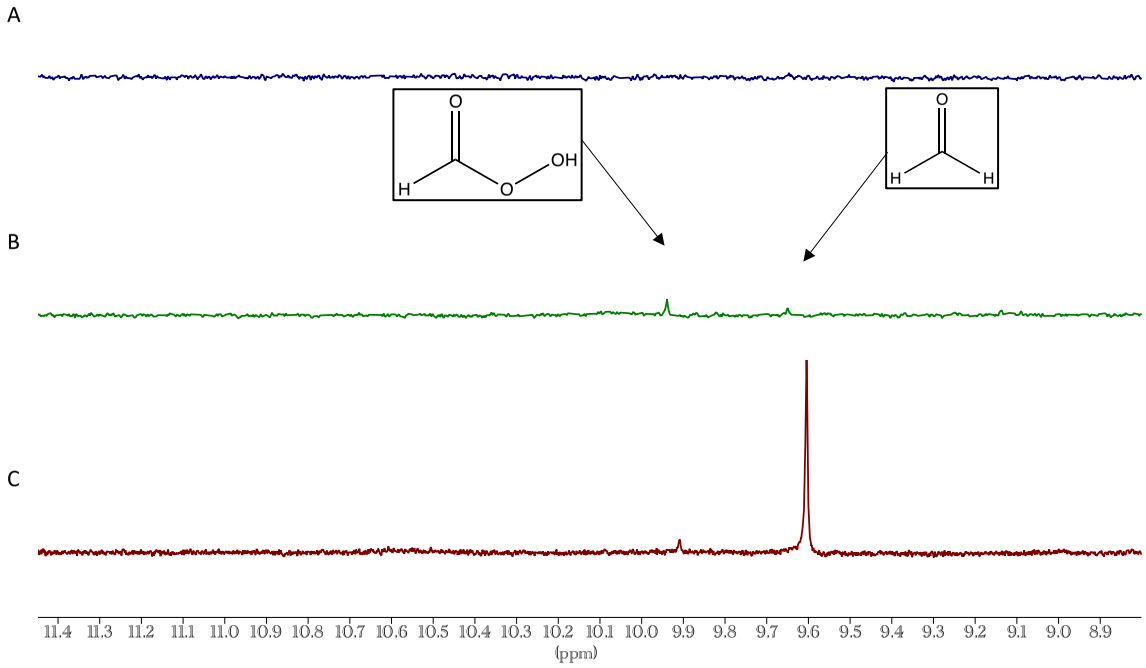

Figure 6. Spike experiment validating formation of formaldehyde. (A) **2** Pd–CH_3 15 mM in CD_3CN; AIBN 54 mM; t = 0 s (B) sample A pressurized with 5 bar O_2 and reaction completed t = 8800 s (C) sample B open to atmosphere and spiked with 5 µL of 37% wt formaldehyde in H_2O with 10 – 15% MeOH. Note the change in chemical shift in spectrum C due to release of 5 bar O_2.

It was suspected that peroxyformic acid (CH_2O_3) may form due to the presence of excess O_2 in this highly oxidative environment. Interestingly, it appeared that the peroxyformic acid peak (CH_2O_3) slowly grew in at later time points as there is a slight decrease in peak area associated with the formaldehyde peak, indicating side oxidation reactions.

It was suspected that if peroxyformic acid formed then there was potential for the formation of formic acid (HCOOH, δ 8.03). An attempt at an analogous spike experiment with formic acid (HCOOH) was performed (data not shown). Unfortunately, the formic acid peak (HCOOH) that grew in upon spiking was overlapped with an existing aromatic peak, thus, this spiking experiment was inconclusive.

2.2.3 Kinetic Rate Law

A mechanistic investigation was carried out to understand the reactivity of **2** with O_2 in the presence of AIBN (**Scheme 16**). The reaction mechanism for the oxidation of **2** was suspected to follow a radical mediated reaction similar to a previous study by Boisvert et al.[9] AIBN was selected as a temperature sensitive radical initiator to ensure replicable initiation of radicals utilizing high-temperature VT-NMR to study the kinetics of the reaction and elucidate a mechanism. By tracking the reactivity over time, a rate law may be derived for **Equation 1**.[21]

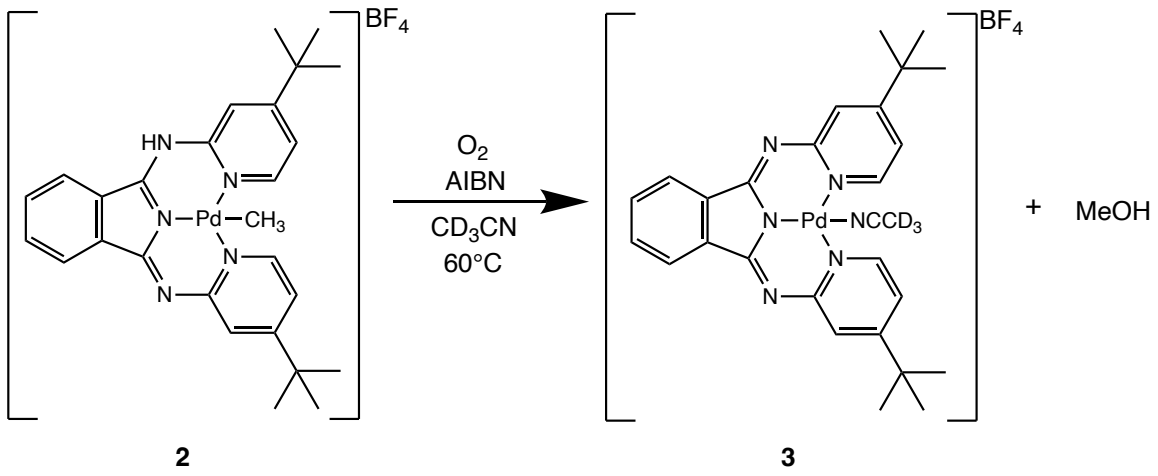

Scheme 16. Reaction of **2** with O_2 in the presence of AIBN to be kinetically investigated to experimentally derive a kinetic rate law.

$$\text{Rate} = \frac{-d\,[^{H}(BPI)Pd^{II}(Me)][BF_4]}{dt} \qquad \textbf{(Eq 1)}$$

A kinetic investigation in CD_3CN was carried out by exposing **2** to an excess of O_2 and AIBN at 333 K. Due to the complexity of the aromatic region in the ^1H NMR spectrum as **2** converts to **3**, the disappearance of the Pd–CH_3 resonance of **2** was tracked

to determine reactivity progress. O_2, AIBN, and **2** were selected as important species to study in experimentally deriving a rate law for the selective oxidation.

2 and AIBN were kept at constant concentrations (Pd–CH_3 = 8.3 – 9.6 mM, AIBN = 51 - 62 mM) while the pressure of O_2 loaded into the J Young NMR tube was varied (2.5 bar, 5 bar, 7 bar) to determine the kinetic dependance of the reaction (**Scheme 15**) on O_2 (**Figure 7**). The disappearance of **2** over time was not observed to change with varying pressurization of O_2; therefore, a zero order dependance on O_2 is concluded for the selective oxidation (**Figure 7**).

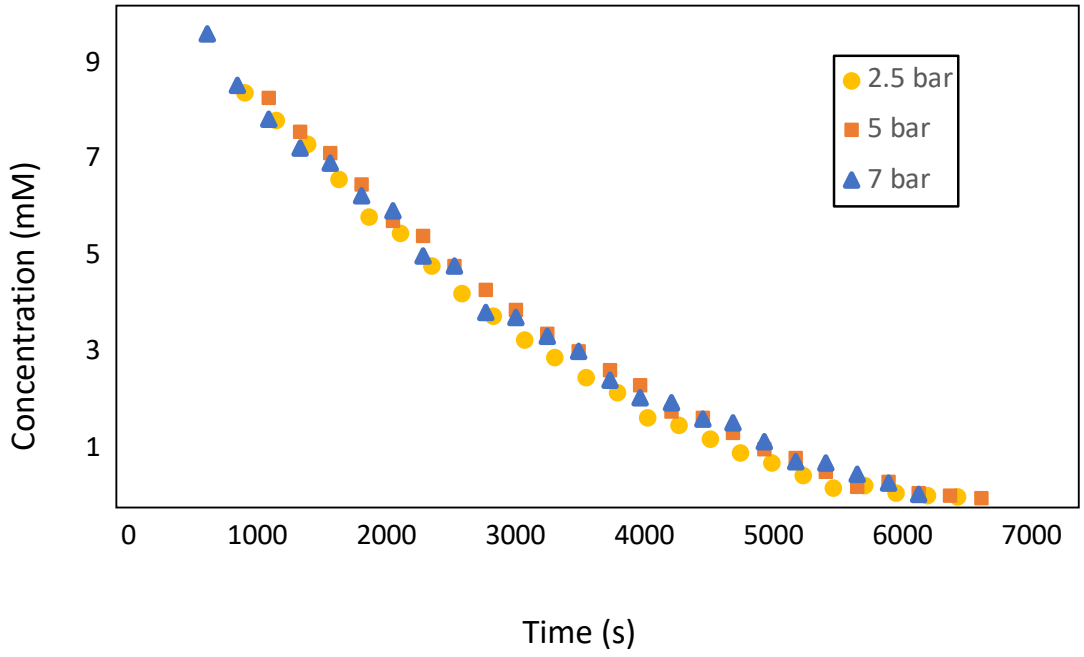

Figure 7. Zero order dependence on O_2 for Pd–CH_3 = 8.3 – 9.6 mM; AIBN = 51 - 62 mM; varying pressurization of O_2.

The rate of the disappearance of **2** tracked with the Pd–CH_3 resonance found in **Scheme 7** was manipulated to determine the best kinetic fitting that models the disappearance of starting material. Experimentally, it was determined that there was a one-half order dependance on **2** (**Figure 8**).

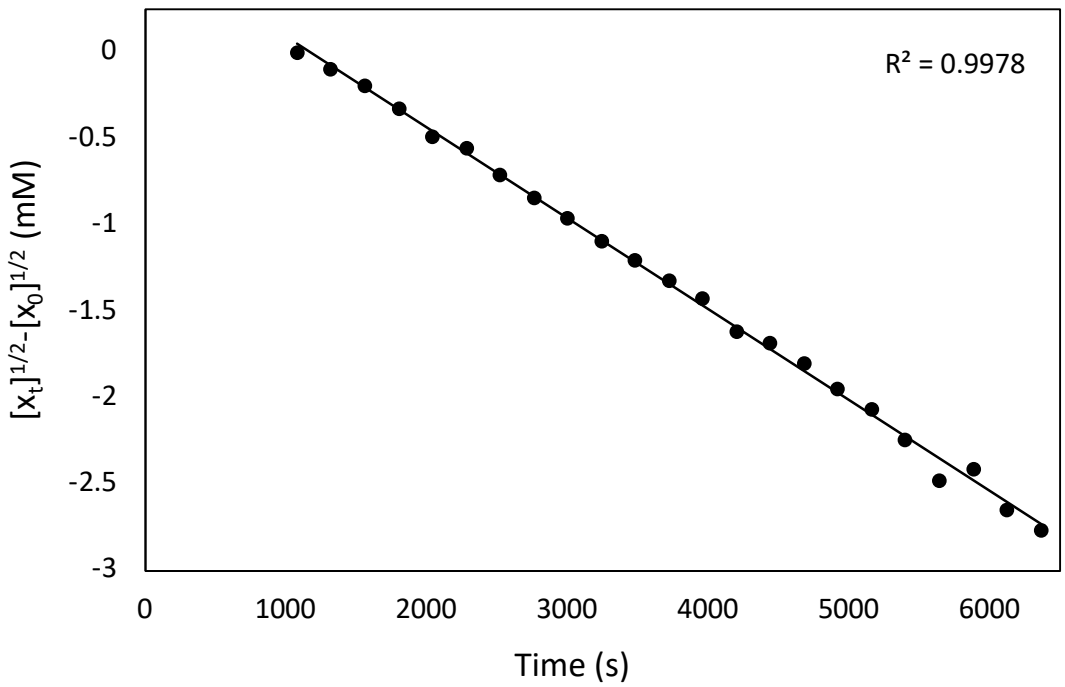

Figure 8. ½ order dependence on **2** for Pd–CH_3 = 8.3 mM; O_2 = 5 bar; AIBN = 51 mM.

This one-half order kinetic fitting had the highest correlation coefficient when fitted linearly as compared to alternative fittings that were applied to rationalize the dependance on **2** (**Figure 9**). Both the first order (**Figure 9A**) and the second order (**Figure 9B**) fitting of the dependance on **2** resulted in obviously nonlinear fits with poor correlation coefficients thus supporting the one-half order dependance on **2** (**Figure 8**).

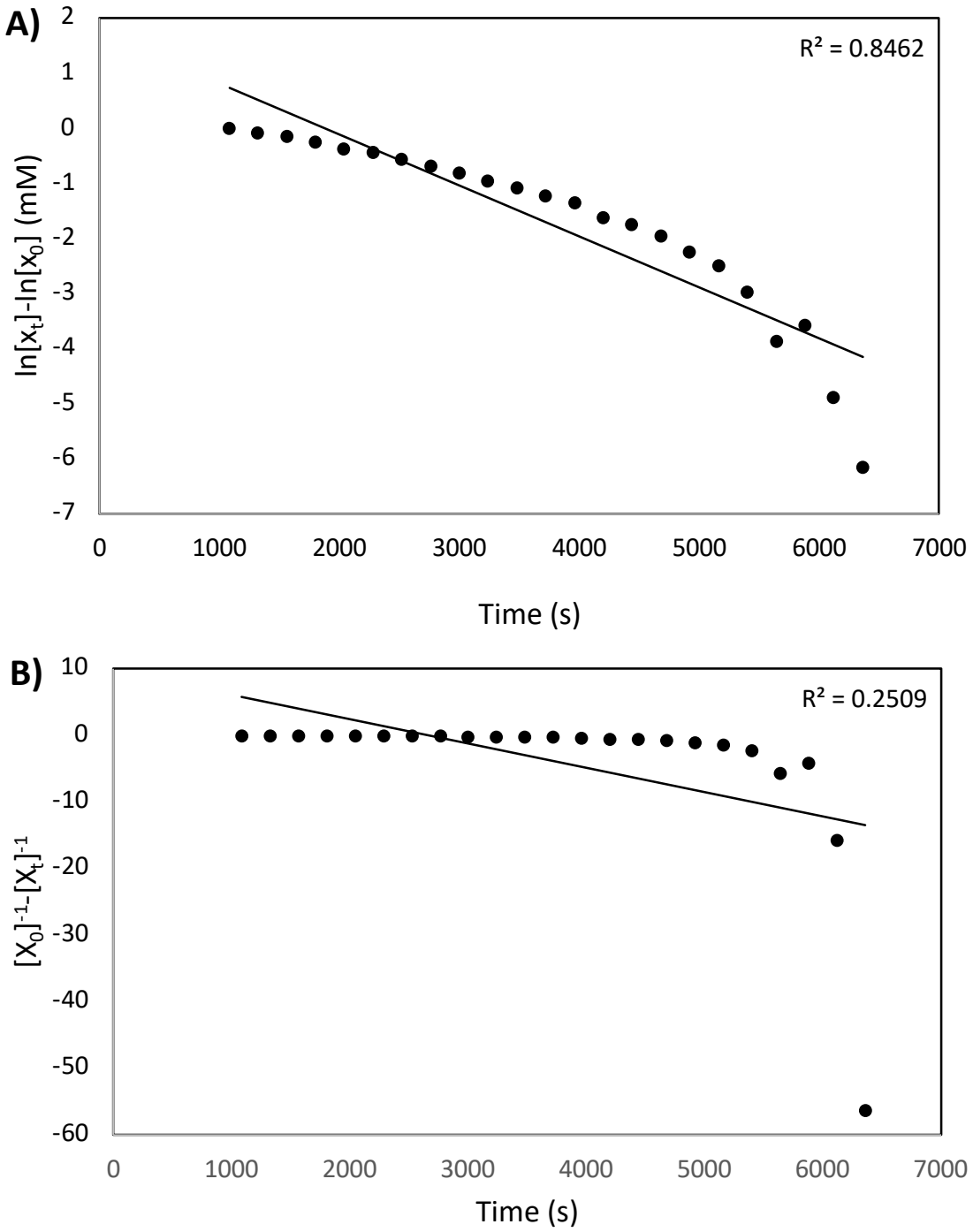

Figure 9. Alternative fittings for dependence on **2** with Pd–CH_3 = 8.27; O_2 = 5 bar; AIBN = 51 mM. (A) 1st order fitting; (B) 2nd order fitting.

The dependance on AIBN was determined similarly to the dependance of O_2. The molar equivalents of AIBN added to the reaction were varied while keeping the concentration of **2** and the pressure of O_2 constant (Pd–CH_3 = 6.9 - 8.5 mM, O_2 = 5 bar) (**Figure 10**). A one-half order dependance on AIBN for the oxidation reaction was determined as this fitting resulted in the highest correlation coefficient and demonstrated a linear relationship (**Figure 10**).

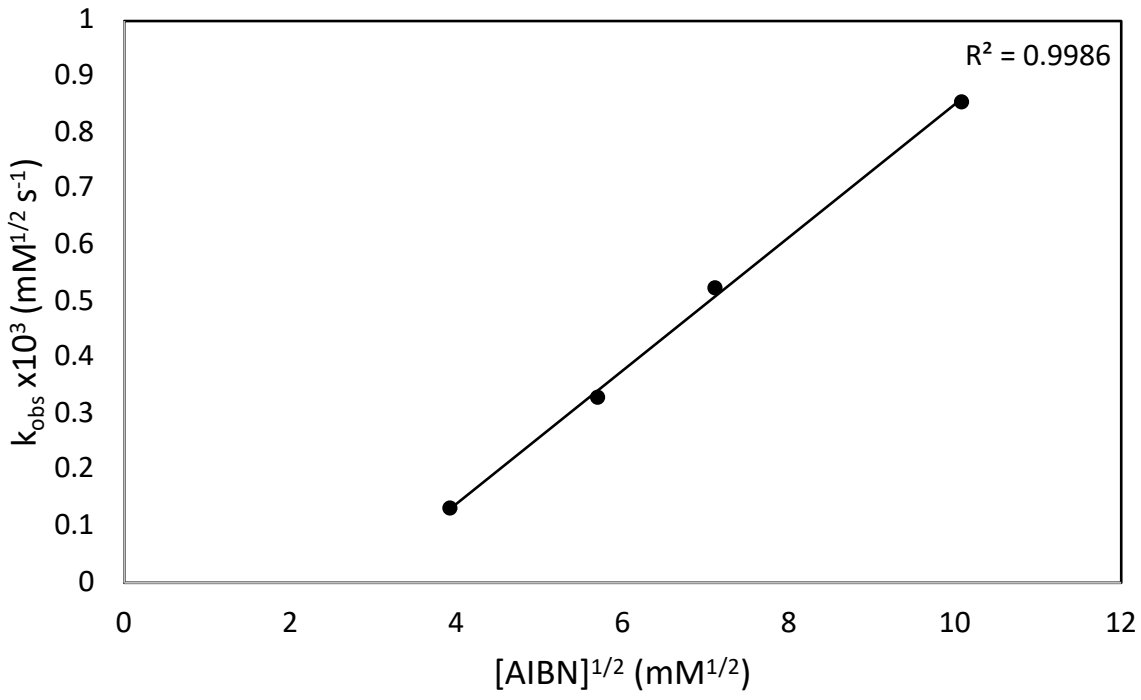

Figure 10. ½ order dependence on AIBN for Pd–CH_3 = 6.9– 8.5 mM; O_2 = 5 bar.

An alternative fitting of first order for AIBN was performed (**Figure 11**). This alternative fitting had a relatively high correlation coefficient; however, demonstrated a nonlinear relationship with a lower correlation coefficient when compared to the linear one-half order dependance fitting.

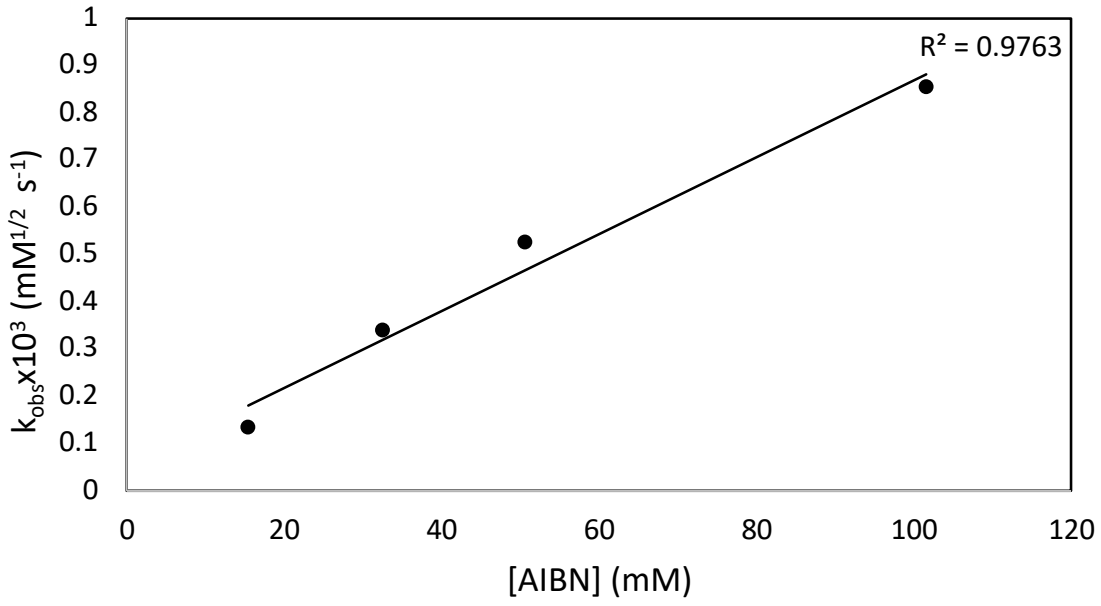

Figure 11. 1st order fitting for AIBN for 2 Pd–CH_3 = 6.9– 8.5 mM; O_2 = 5 bar.

The kinetic investigation experimentally resulted in a preliminary rate law in **Equation 2**. This demonstrated a one-half order dependance on AIBN and **2** contributing to an overall first order reaction. This equation also illustrated the independence of O_2 in the selective oxidation.

$$\text{Rate} = k_{obs}\,[\text{AIBN}]^{1/2}\,[\mathbf{2}]^{1/2}\,[O_2]^0 \qquad \textbf{(Eq 2)}$$

2.2.4 Proposed Mechanism

A similar radical mediated reaction mechanism for the selective oxidation of Pd–CH_3 in **2** was suspected as previously studied for the conversion of [(bipy)Pd(Me)$_2$] to [(bipy)Pd(Me)(OOMe)] by Boisvert et al.[8-9] This mechanism illustrated for the reactivity of **2** with AIBN in the presence of O_2 is detailed below (**Scheme 17**).

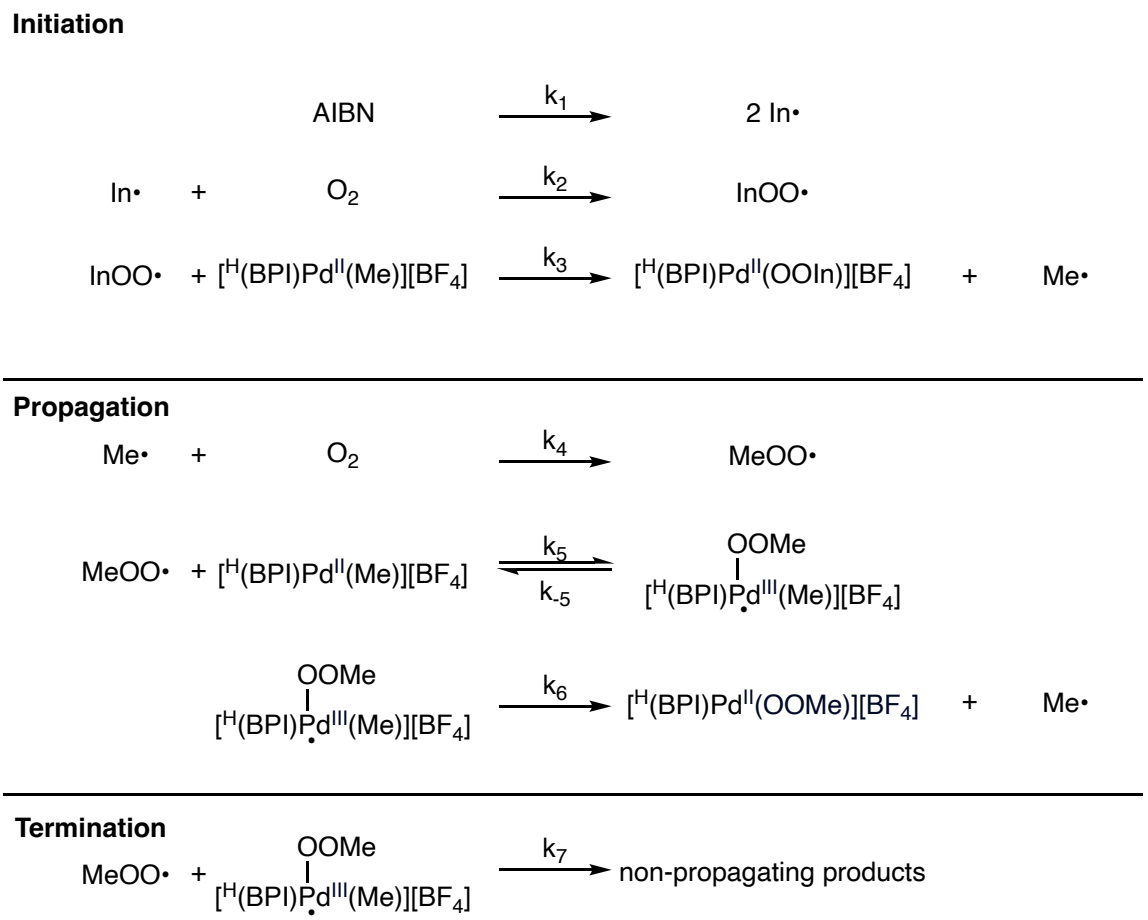

Scheme 17. Proposed mechanism for the reaction of **2** with O_2 utilizing AIBN to form the peroxy-species $[^{H}(BPI)Pd(OOMe)][BF_4]$.

Under steady state conditions, the initiation and termination steps are assumed to occur at the same rate, **Equation 3**. This equation can be rewritten to solve for [MeOO•] thus producing **Equation 4**.

$$k_1\,[AIBN] = k_7\,[^{H}(BPI)Pd^{III}(Me)(OOMe)\bullet][BF_4]\,[MeOO\bullet] \qquad \textbf{(Eq 3)}$$

$$[MeOO\bullet] = \frac{k_1\,[AIBN]}{k_7\,[^{H}(BPI)Pd^{III}(Me)(OOMe)\bullet][BF_4]} \qquad \textbf{(Eq 4)}$$

Assuming that the chains for the radical reaction are long, the steady state approximation can be applied to $[^{H}(BPI)Pd^{III}(Me)(OOMe)\bullet][BF_4]$ for steps 5, -5, and 6 in the mechanism resulting in **Equation 5** (**Scheme 17**). Substitution of **Equation 4** into **Equation 5**

followed by rearrangement to solve for $[^{H}(BPI)Pd^{III}(Me)(OOMe)\bullet][BF_4]$ results in **Equation 6**.

$$[^{H}(BPI)Pd^{III}(Me)(OOMe)\bullet][BF_4] = \frac{k_5\,[^{H}(BPI)Pd^{II}(Me)][BF_4]\,[MeOO\bullet]}{k_{-5} + k_6} \qquad \textbf{(Eq 5)}$$

$$[^{H}(BPI)Pd^{III}(Me)(OOMe)\bullet][BF_4] = \left(\frac{k_1 k_5\,[^{H}(BPI)Pd^{II}(Me)][BF_4]\,[AIBN]}{k_7(k_{-5} + k_6)}\right)^{1/2} \qquad \textbf{(Eq 6)}$$

The consumption of $[^{H}(BPI)Pd^{II}(Me)][BF_4]$ is equal to the production of $[^{H}(BPI)Pd^{II}(OOMe)][BF_4]$ in **Equation 7**. **Equation 8** can be obtained by substituting **Equation 6** into **Equation 7**.

$$\text{Rate} = \frac{-d\,[^{H}(BPI)Pd^{II}(Me)][BF_4]}{dt} = k_6\,[^{H}(BPI)Pd^{III}(Me)(OOMe)\bullet][BF_4] \qquad \textbf{(Eq 7)}$$

$$\text{Rate} = \frac{-d\,[^{H}(BPI)Pd^{II}(Me)][BF_4]}{dt} = \left(\frac{k_1 k_5 k_6^2}{k_7(k_{-5} + k_6)}\right)^{1/2} [^{H}(BPI)Pd^{II}(Me)][BF_4]^{1/2}\,[AIBN]^{1/2} \qquad \textbf{(Eq 8)}$$

This **Equation 8** demonstrates the rate dependance of a one-half order on **2** and AIBN with an overall kinetic rate order of first order. This mechanistic derivation of the rate law is consistent with the experimental rate law determined in **Equation 2**. The proposed mechanism may explain the selective oxidation of the Pd–Me complex thus obtaining a Pd–OOMe species as the product of this step (**Scheme 17**).

In the experimental results, the presence of a Pd–OOMe species was not observed but rather the production of mainly MeOH, MeOOH, and **3** (**Figure 2**; **Figure 4**). This may be rationalized as the formation of the Pd–OOMe species is the slow step of the reaction and thus the kinetics are explained through this mechanism (**Scheme 17**). The further functionalization of free small carbon oxidized species such as MeOH is assumed to be a fast process and thus no kinetic dependance is observed in this kinetic

investigation. Further investigation into the mechanism for the functionalization of MeOH will have to be carried out.

3. Conclusion & Future Directions

The charged palladium analogue to a previous complex of interest was prepared and the synthesis was optimized.[10] This complex was suspected to be able to react with elemental dioxygen to selectively oxidize the Pd–Me similar to previous works.[9-10,14] A mechanistic investigation was performed to experimentally derive a kinetic rate law for the reactivity of **2** with O_2 utilizing the radical initiator AIBN in CD_3CN. This experimental rate law in **Equation 1** was consistent with previous studied radical mediated selective oxidations and thus a mechanism was proposed for this reactivity (**Scheme 17**).[9-10] Utilizing this proposed mechanism, a kinetic rate law was derived in **Equation 7** which is consistent with experimental results.

2 is a novel complex in the catalytic cycle of interest (**Scheme 3**) as reactivity resulted in the functionalize or release of free MeOH.[9-10] In previous works involving the BPI framework, the selective oxidation of Pd–Me resulted in a stable metal–OOMe species that does not liberate functionalized MeOH or MeOOH.[9-10] In this study, liberated MeOH and MeOOH was observed (**Figure 4**). This functionalization was independent of the kinetic rate law determined experimentally and theoretically as this was expected to be a rapid step and thus the kinetics are dependent on the slow oxidation step resulting in the formation of $[^{H}(BPI)Pd(OOMe)][BF_4]$.

An additional investigation into the fate of small carbon species produced by the reaction of **2** with O_2 is of interest. Potential ^{13}C labeling of the activated methane may be utilized to track and confirm the destiny of the small carbon species produced via

$^{13}C\{^{1}H\}$ NMR spectroscopy. Similarly, GC-MS may also be utilized to identify and quantify the small carbon species produced from this selective oxidation reaction.

Further investigation into **3** is of interest to see if methane may be activated or complexed to the Pd metal center again to complete the catalytic cycle in **Scheme 3**. An additional photolytic investigation is of interest considering preliminary evidence of **2** being capable of reacting with O_2 at room temperature in the absence of a radical initiator like AIBN. This is consistent with previous photolytic work by Ho et al.[14] A photocatalyzed selective oxidation is of interest as this embraces the principals of green chemistry capable of performing the selective oxidation under ambient conditions open to air and light.

4. Materials and Methods

4.1 Physical Measurements

^{1}H NMR spectra were collected using a Bruker AVIII Bio 500 MHz spectrometer with a 5 mm BBFO probe unless otherwise noted. All ^{19}F NMR spectra were collected using a Bruker AVIII Bio 376 MHz spectrometer with a 5 mm BBFO probe. DOSY NMR spectrum was collected with a Bruker 400 MHz spectrometer. Chemical shifts were referenced to residual solvent. s = singlet, d = doublet, dd = doublet of doublets, m = multiplet.

4.2 Synthetic and Characteristic Protocol

All reactions and manipulations were performed under an inert atmosphere (N_2) using standard Schlenk techniques or in a vacuum atmosphere dry box equipped with oxygen and moisture purifier systems. Glassware was dried overnight at 60°C prior to use. $(CD_3)_3CO$, CD_3CN, C_6D_6, and $CDCl_3$ were purchased anhydrous and stored over 4 Å molecular sieves before use. CD_3CN utilized in kinetics was purchased anhydrous, rigorously dried with CaH_2 under vacuum, transferred to a Schlenk tube, and stored over 4 Å molecular sieves then passed over celite prior to use.

4.3 Organic BPI Framework

4.3.1 Synthesis of 4-(tert-butyl)pyridine-N-oxide

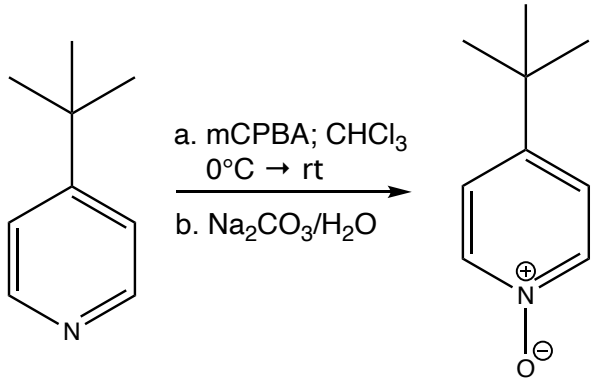

Scheme 18. Synthetic scheme for 4-(*tert*-butyl)pyridine-N-oxide.

Preparation followed standard literature procedures open to air (**Scheme 18**).[18] 4-(*tert*-butyl)pyridine (3.0 g, 22.2 mmol) was added to a round bottom flask equipped with a magnetic stir bar and containing 60 mL of $CHCl_3$. The resultant solution was chilled with an ice bath to 0°C. *meta*-Chloroperoxybenzoic acid (*m*CPBA; 6.56 g; 26.6 mmol) suspended in $CHCl_3$ (60 mL) was added in portions to the chilled, stirring reaction mixture over the course of 20 min. The reaction turned a cloudy white and was allowed to come to room temperature after which it was stirred overnight. The resultant homogenous reaction mixture was quenched with an excess of Na_2CO_3, extracted with $CHCl_3$, and dried with $MgSO_4$ and *in vacuo*. 4-(*tert*-butyl)pyridine-*N*-oxide was collected as a yellow solid (3.32 g, 21.9 mmol, 99% yield). ^{1}H NMR (500 MHz, $CDCl_3$) confirmed product formation and purity δ 8.16 (d, J = 7.2 Hz, 2H), δ 7.27 (d, 2H), δ 1.31 (s, 9H) (**Figure S1**).

4.3.2 Synthesis of 2-amino-4-(tert-butyl)pyridine

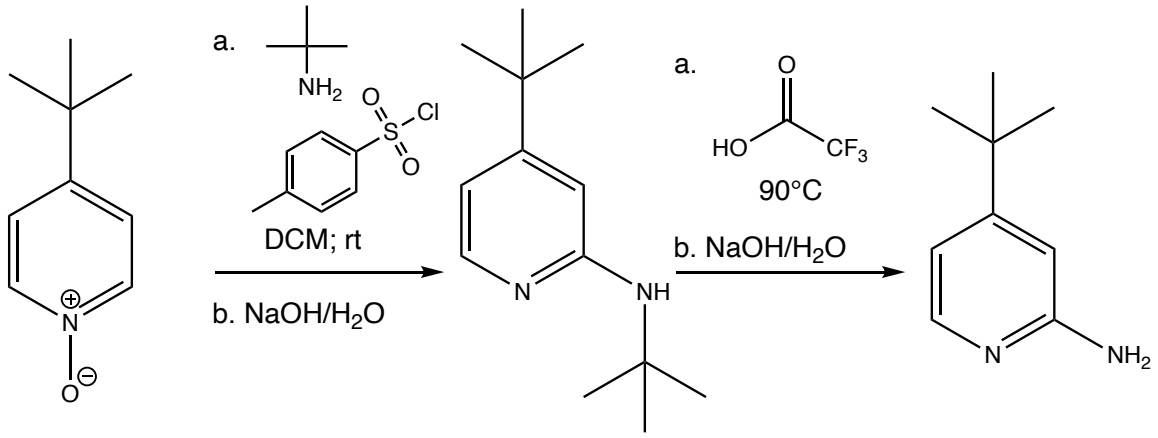

Scheme 19. Synthetic scheme for 2-amino-4-(*tert*-butyl)pyridine.

Preparation was modeled after standard literature procedures open to air (**Scheme 19**).[18] 4-(*tert*-butyl)pyridine-*N*-oxide (1.75 g, 11.6 mmol) was massed into a reaction flask equipped with a magnetic stir bar and DCM (150 mL). (*tert*-butyl)amine (6.08 mL, 57.9 mmol) was added forming a cloudy yellow solution. TsCl (4.41 g, 23.1 mmol) was massed and added to the reaction flask over 1 hr. The reaction was stirred overnight and observed to be incomplete the next morning as verified by ^{1}H NMR. TsCl (2.21 g, 11.6 mmol) was recharged into the reaction flask over 20 min period. Incomplete conversion was observed by ^{1}H NMR spectroscopy by taking an aliquot, drying *in vacuo*, then dissolving in $CDCl_3$ with a spike of triethylamine (TEA). (*tert*-butyl)amine (6.06 mL, 57.9 mmol) was added along with a slow addition of TsCl (4.41 g, 23.1 mmol) over 45 min. The reaction was stirred overnight. Incomplete conversion was observed by ^{1}H NMR; therefore, (*tert*-butyl)amine (6.06 mL, 57.9 mmol) was added along with a slow addition of TsCl (4.41 g, 23.1 mmol) over 30 min. The reaction was completed and worked up with an aqueous NaOH solution (1.04 M) with 2 extractions (50 mL) followed

by 3 extractions with DCM (75 mL). The resulting organic solution was dried with $MgSO_4$ and *in vacuo*. Organic solids were dissolved with warm EtOAc and allowed to come to room temperature to which hexanes were added (225 mL) and the recrystallization was allowed to occur over 2 days. A vacuum filtration was performed to extract product in the supernatant which was then dried *in vacuo*. Dried filtrate containing the *tert*-butyl protected aminated intermediated was then added to a round bottom flask equipped with a magnetic stir bar and TFA fitted with a condenser. The reaction flask was heated to 90°C and allowed to react overnight. The reaction mixture was quenched with an aqueous NaOH solution (100 mL, 3.65 M) and extracted with 3 additions of DCM (100 mL) and dried with $MgSO_4$ and *in vacuo*. The resulting oil was dry loaded onto a silica gel column equilibrated with 1:1 EtOAc : hexanes, eluted, and dried *in vacuo*. 2-amino-4-(*tert*-butyl)pyridine was collected as a yellow solid (0.9751 g, 6.49 mmol, 56% yield). ^{1}H NMR confirmed product formation (500 MHz, $CDCl_3$): δ 7.94 (d, J = 5.6 Hz, 1H), δ 6.66 (dd, J = 5.53, 1.7 Hz, 1H), δ 6.48 (s, 1H), δ 4.48 (s, 2H), δ 1.25 (d, 9H) (**Figure S2**).

4.3.3 Synthesis of 1,3-bis(2-(4-tert-butyl)pyridylimino)isoindole (BPI)

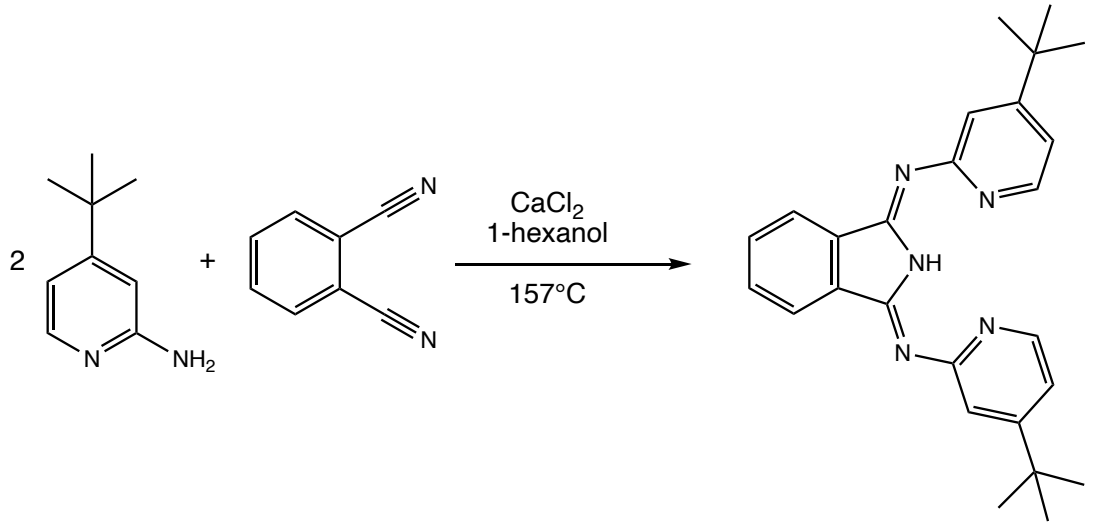

Scheme 20. Synthetic scheme for BPI.

Preparation of BPI was modeled after standard literature procedures (**Scheme 20**).[19] 2-amino-4-(*tert*-butyl)pyridine (0.5 g, 3.33 mmol); 1,2-dicyanobenzene (0.2133 g, 1.66 mmol); calcium chloride ($CaCl_2$, 0.0370 g, 0.33 mmol) were massed into a round bottom flask equipped with a magnetic stir bar and 1-heaxanol (10 mL) fitted with a condenser and back filled with N_2. The reaction was stirred at reflux (157°C) for 3 days. The resulting brown solution was dried *in vacuo* and the brown solids were transferred to a sintered glass frit with H_2O. The solids were triturated with cold hexanes followed by a rinse of DCM. The yellow filtrate was dried, and a yellow solid of BPI was collected (0.471 g, 1.15 mmol, 69% yield) and stored in a glovebox. ^1H (500 MHz; $CDCl_3$): δ 13.97 (s, 1H), δ 8.51 (d, J = 5.3 Hz, 2H), δ 8.08 (dd, J = 5.7, 3.1 Hz, 2H), δ 7.65 (dd, J = 5.6, 3.0 Hz, 2H), δ 7.47 (s, 2H), δ 7.12 (dd, J = 5.5, 1.9 Hz, 2H), δ 1.37 (s, 18H) (**Figure S3**).

4.4 Inorganic Pd Framework

4.4.1 Synthesis of [(TMEDA)Pd(Cl)$_2$]

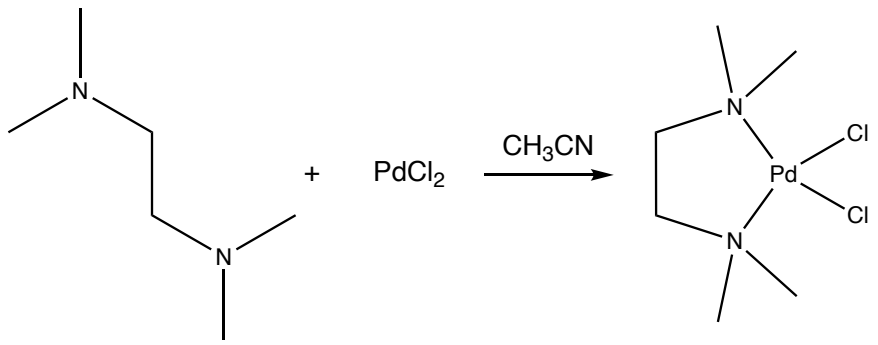

Scheme 21. Synthetic scheme for [(TMEDA)Pd(Cl)$_2$].

Preparation of [(TMEDA)Pd(Cl)$_2$] followed standard literature procedures (**Scheme 21**).[20] Palladium chloride ($PdCl_2$, 6.0 g, 33.8 mmol) was massed into a Schlenk flask equipped with a magnetic stir bar and back filled with N_2. Dry acetonitrile (CH_3CN, 200 mL) was cannula transferred into the reaction flask. The red suspension was left to react overnight. The orange suspension was heated to reflux (82°C) fitted with a condenser until all precipitate dissolved (1 hr). The yellow solution was allowed to cool (1 hr) and N,N,N′,N′-tetramethylethylenediamine (TMEDA, 6 mL, 40.0 mmol) was added via a syringe. The resulting reaction mixture was allowed to stir (1 hr) before being opened to air, filtered with 3 Et_2O rinses (25 mL), and dried *in vacuo*. Yellow [(TMEDA)Pd(Cl)$_2$] was collected (9.476 g; 32.5 mmol; 96% yield). ^{1}H NMR (500 MHz; $CDCl_3$): δ 2.83 (s, 12H), δ 2.69 (s, 4H) (**Figure S4**).

4.4.2 Synthesis of [(TMEDA)Pd(Me)$_2$]

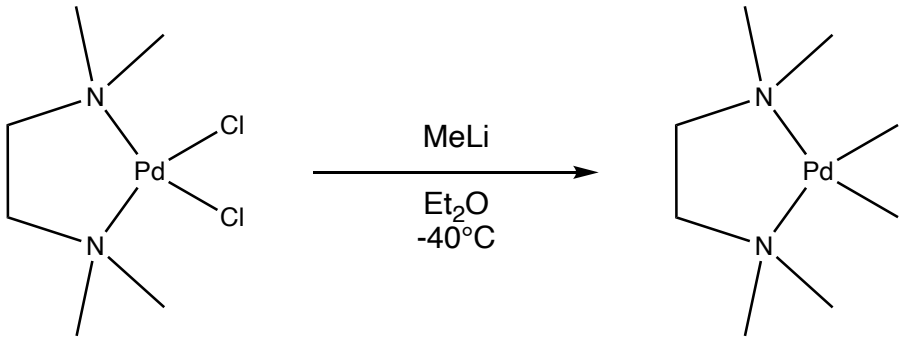

Scheme 22. Synthetic scheme for [(TMEDA)Pd(Me)$_2$].

Preparation of [(TMEDA)Pd(Me)$_2$] followed standard literature procedures (**Scheme 22**).[20] [(TMEDA)Pd(Cl)$_2$] (1.0 g, 3.43 mmol) was massed into Schlenk flask equipped with a magnetic stir bar and back filled with N_2 and chilled to -40°C. Et_2O (13 mL) was cannula transferred to the reaction flask which was allowed to stir followed by an addition of MeLi solution (2.76 mL, 3.1 M in diethoxymethane, 8.56 mmol). The orange solution was allowed to come to 0°C and stirred to react for 1 hr becoming a brown solution. The reaction was allowed to come to room temperature before degassed H_2O was cannula transferred to quench. The product was extracted with 3 additions of Et_2O (20 mL) and dried *in vacuo* before taken up in benzene and filtered over a sintered glass frit. The clear filtrate was dried *in vacuo*, and the white powder was taken up in pentane and collected over a sintered glass frit and further dried *in vacuo*. Solid white [(TMEDA)Pd(Me)$_2$] was collected (0.452 g, 1.8 mmol, 52% yield) and stored at -30°C in a glovebox. ^{1}H NMR (500 MHz; $(CD_3)_2CO$): δ 2.53 (s, 4H), δ 2.37 (s, 12H), δ -0.38 (s, 6H) (**Figure S5**).

4.5 Preparation of Pd catalyst

4.5.1 Synthesis of [(BPI)Pd(Me)]

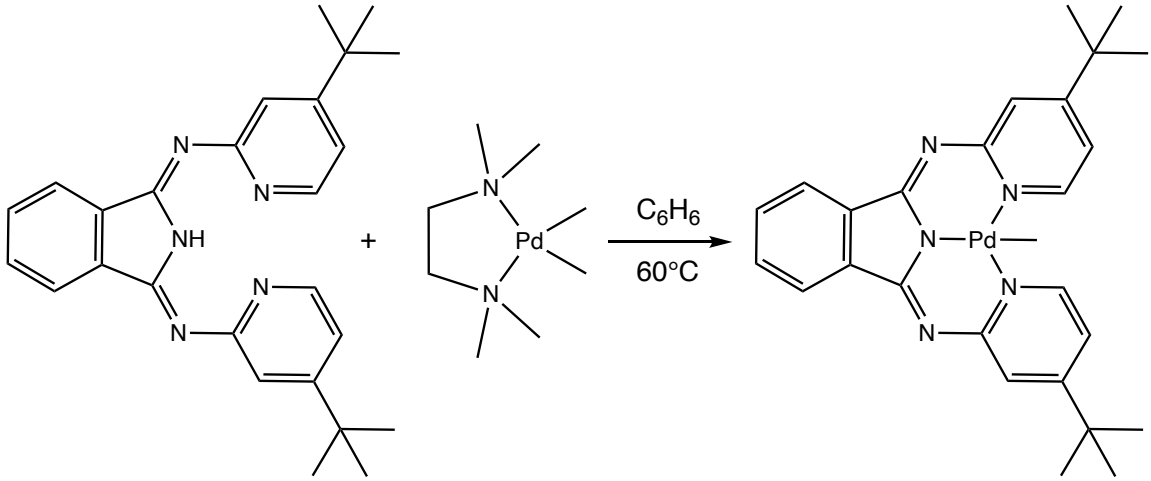

Scheme 23. Synthetic scheme for [(BPI)Pd(Me)].

In the glovebox, BPI (100 mg, 0.242 mmol) and [(TMEDA)Pd(Me)$_2$] (61 mg, 0.242 mmol) were massed into a Schlenk flask equipped with a magnetic stir bar and dissolved in benzene (6 mL). The yellow solution was stirred overnight at 60°C under N_2 fitted with a condenser (**Scheme 23**). The red solution was dried *in vacuo* and a red powder of **1** was collected (121.8 mg, 94% yield) and stored in the glovebox. ^{1}H NMR (400 MHz; C_6D_6): δ 8.70 (d, J = 6.6 Hz, 2H), δ 8.30 (dd, J = 5.4, 3.1 Hz, 2H), δ 7.79 (d, J = 2.5 Hz, 2H), δ 7.27 – 7.19 (m, 2H), δ 6.45 (dd, J = 6.5, 2.5 Hz, 2H), δ 1.02 (s, 24H), δ 0.30 (s, 3H) (**Figure S6**).

4.5.2 Synthesis of [^{H}(BPI)Pd(Me)][BF$_4$]

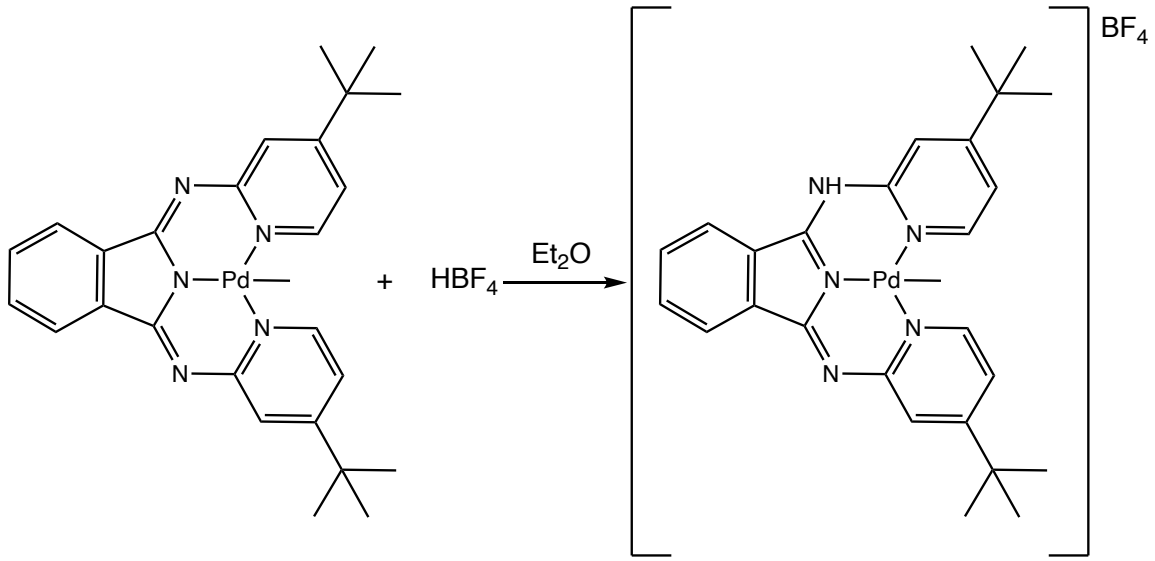

Scheme 24. Synthetic scheme for [^{H}(BPI)Pd(Me)][BF$_4$].

In the glovebox, **1** (100 mg, 0.188 mmol) was massed into an Erlenmeyer flask and dissolved in Et_2O (40 mL). Fluoroboric acid (HBF_4, 33.015 mg, 50-55% w/w in Et_2O, 0.188 mmol) was massed into a separate Erlenmeyer flask and diluted with Et_2O to make a HBF_4 solution (9.4 M HBF_4). The HBF_4 solution was added dropwise over 20 minutes into the Erlenmeyer flask containing the red solution of **1**. Upon addition of HBF_4 solution, a yellow precipitate of **2** crashed out (**Scheme 24**). **2** was collected on a sintered glass frit and rinsed with Et_2O (2 mL) to produce a yellow powder (72.2 mg,m 62% yield) stored in a glovebox. ^{1}H NMR (500 MHz; CD_3CN): δ 8.66 (d, J = 6.4 Hz, 2H), δ 8.18 (s, 2H), δ 7.85 (s, 2H), δ 7.79 (s, 2H), δ 7.46 (d, J = 6.4 Hz, 2H), δ 1.41 (s, 18H), δ 0.87 (s, 3H) (**Figure S7**). ^{19}F{^{1}H} NMR (376 MHz; CD_3CN): δ -151.61 (d, 4F) (**Figure S8**).

4.6 DOSY

Complex **2** was opened to air and was dissolved in non-rigorously dried CD_3CN to conduct a 2D NMR analysis of size. DOSY NMR collected with Bruker's "1edbpg2s" program with the gradient strength (g), diffusion time (Δ), and diffusion gradient (δ) optimized according to the Bruker DOSY Manuel (**Table 1**).[22] A gradient ramp from g = 2% to g = 95% with 16 linear steps (TD[F1]) was utilized with optimized Δ (D20 = 50 ms) and δ (P30 = 1.0 ms) for complex **2**.

Table 1. The acquisition parameters for DOSY of **2**.

PULPROG:	ledbpgp2s	TD[F2]:	65K	TD[F1]:	16
NS:	16	DS:	2	D20	50 ms
D21	5 ms	P30:	1.0 ms	P19	0.6 ms
GPZ6:	100%	GPZ7:	-17.13%	GPZ8:	-13.17%

The 2D DOSY spectra were processed with a Bayesian DOSY Transform (BDT) utilizing MestReNova version 14.2.3 with a BDT resolution factor of 1.00, a single repetition, and 128 points in the diffusion dimension.

4.7 Kinetics

4.7.1 Rate Determination Kinetics

Implementing RPKA, the disappearance of the Pd–Me resonance in the aliphatic region of the ^{1}H NMR spectrum of **2** allowed for the tracking of the disappearance of the reactant **2** and thus appearance of product **3** to create a concentration of reactant **2** versus time plot to determine kinetics with respect to varied reactant conditions.[21]

All preparations were carried out under an inert atmosphere. Stock solutions of complex **2** (40.3 mM), AIBN (0.944 M), and Mes (64.52 mM) were prepared in rigorously dried and filtered CD_3CN and stored at room temperature. Appropriate amounts of stock solutions were transferred to a J Young NMR tube with a micropipette and the reaction solution was topped off with CD_3CN to a final volume of 0.5000 mL. A constant amount of Mes stock (62.41 μL; 64.52 mM) was used for all kinetic trials thus the concentration of the internal standard Mes in the final reaction mixture was known (8.054 mM) to quantify the reaction progress. An initial spectrum of each sample under N_2 (1 bar) was collected to ensure that there were no impurities present prior to reacting. The J Young tube was then freeze-pump-thawed three times before pressurization of a certain amount of oxygen (2.5 - 7 bar) at room temperature. The sample was then placed into the NMR spectrometer preheated to 333 K and a ^{1}H pseudo 2D kinetic experiment with a pulse angle of 30 degrees was collected with 1 scan every 4 minutes to track reaction progress. The reaction was followed and data collected for at least 3 half-lives.

4.7.2 Spike Experiments

After completion of a kinetic trial, the sample was allowed to come to room temperature before being opened to air to release the pressurized O_2. The appropriate spike was added, and the J Young was sealed with a final ^1H NMR spectrum being collected at room temperature with atmosphere (1 bar air). A formaldehyde solution (5 μL, 37% w/w formaldehyde in H_2O with 10-15% methanol) was spiked to probe the formation of formaldehyde. Methanol (0.3 μL) was spiked to probe the formation of methanol.

5. References

(1) *Energy Statistics Data Browser – Data Tools - IEA*. https://www.iea.org/data-and-statistics/data-tools/energy-statistics-data-browser?country=WORLD&fuel=Energy%20supply&indicator=TESbySource (accessed 2022-09-26).

(2) Caballero, A.; Pérez, P. J. Methane as Raw Material in Synthetic Chemistry: The Final Frontier. *Chem. Soc. Rev.* **2013**, *42* (23), 8809. https://doi.org/10.1039/c3cs60120j.

(3) *Methane emissions*. https://energy.ec.europa.eu/topics/oil-gas-and-coal/methane-emissions_en (accessed 2023-04-14).

(4) Olah, G. A. Beyond Oil and Gas: The Methanol Economy. *Angew. Chem. Int. Ed.* **2005**, *44* (18), 2636–2639. https://doi.org/10.1002/anie.200462121.

(5) da Silva, M. J. Synthesis of Methanol from Methane: Challenges and Advances on the Multi-Step (Syngas) and One-Step Routes (DMTM). *Fuel Process. Technol.* **2016**, *145*, 42–61. https://doi.org/10.1016/j.fuproc.2016.01.023.

(6) *12 Principles of Green Chemistry*. American Chemical Society. https://www.acs.org/greenchemistry/principles/12-principles-of-green-chemistry.html (accessed 2023-02-03).

(7) Gunsalus, N. J.; Koppaka, A.; Park, S. H.; Bischof, S. M.; Hashiguchi, B. G.; Periana, R. A. Homogeneous Functionalization of Methane. *Chem. Rev.* **2017**, *117* (13), 8521–8573. https://doi.org/10.1021/acs.chemrev.6b00739.

(8) Zeitler, H. E.; Phearman, A. S.; Gau, M. R.; Carroll, P. J.; Cundari, T. R.; Goldberg, K. I. Metal–Ligand–Anion Cooperation in C–H Bond Formation at Platinum(II). *J. Am. Chem. Soc.* **2022**, *144* (32), 14446–14451. https://doi.org/10.1021/jacs.2c05096.

(9) Boisvert, L.; Denney, M. C.; Hanson, S. K.; Goldberg, K. I. Insertion of Molecular Oxygen into a Palladium(II) Methyl Bond: A Radical Chain Mechanism Involving Palladium(III) Intermediates. *J. Am. Chem. Soc.* **2009**, *131* (43), 15802–15814. https://doi.org/10.1021/ja9061932.

(10) Zeitler, H. E.; Kaminsky, W. A.; Goldberg, K. I. Insertion of Molecular Oxygen into the Metal–Methyl Bonds of Platinum(II) and Palladium(II) 1,3-Bis(2-Pyridylimino)Isoindolate Complexes. *Organometallics* **2018**, *37* (21), 3644–3648. https://doi.org/10.1021/acs.organomet.8b00573.

(11) Grice, K. A.; Goldberg, K. I. Insertion of Dioxygen into a Platinum(II)−Methyl Bond To Form a Platinum(II) Methylperoxo Complex. *Organometallics* **2009**, *28* (4), 953–955. https://doi.org/10.1021/om8011272.

(12) Petersen, A. R.; Taylor, R. A.; Vicente-Hernández, I.; Mallender, P. R.; Olley, H.; White, A. J. P.; Britovsek, G. J. P. Oxygen Insertion into Metal Carbon Bonds: Formation of Methylperoxo Pd(II) and Pt(II) Complexes via Photogenerated Dinuclear Intermediates. *J. Am. Chem. Soc.* **2014**, *136* (40), 14089–14099. https://doi.org/10.1021/ja5055143.

(13) Look, J. L.; Wick, D. D.; Mayer, J. M.; Goldberg, K. I. Autoxidation of Platinum(IV) Hydrocarbyl Hydride Complexes To Form Platinum(IV) Hydrocarbyl Hydroperoxide Complexes. *Inorg. Chem.* **2009**, *48* (4), 1356–1369. https://doi.org/10.1021/ic801216r.

(14)Ho, S. K. Y.; Lam, F. Y. T.; de Aguirre, A.; Maseras, F.; White, A. J. P.; Britovsek, G. J. P. Photolytic Activation of Late-Transition-Metal–Carbon Bonds and Their Reactivity toward Oxygen. *Organometallics* **2021**, *40* (24), 4077–4091. https://doi.org/10.1021/acs.organomet.1c00487.
(15)Goldman, A. S.; Goldberg, K. I. Organometallic C-H Bond Activation: An Introduction. **2004**.
(16)Stahl, S. S. Palladium Oxidase Catalysis: Selective Oxidation of Organic Chemicals by Direct Dioxygen-Coupled Turnover. *Angew. Chem. Int. Ed.* **2004**, *43* (26), 3400–3420. https://doi.org/10.1002/anie.200300630.
(17)Taylor, R. A.; Law, D. J.; Sunley, G. J.; White, A. J. P.; Britovsek, G. J. P. Towards Photocatalytic Alkane Oxidation: The Insertion of Dioxygen into a Platinum(II)-Methyl Bond. *Angew. Chem. Int. Ed.* **2009**, *48* (32), 5900–5903. https://doi.org/10.1002/anie.200806187.
(18)Yin, J.; Xiang, B.; Huffman, M. A.; Raab, C. E.; Davies, I. W. A General and Efficient 2-Amination of Pyridines and Quinolines. *J. Org. Chem.* **2007**, *72* (12), 4554–4557. https://doi.org/10.1021/jo070189y.
(19)Langlotz, B. K.; Lloret Fillol, J.; Gross, J. H.; Wadepohl, H.; Gade, L. H. Living Radical Polymerization of Acrylates Mediated by 1,3-Bis(2-Pyridylimino)Isoindolatocobalt(II) Complexes: Monitoring the Chain Growth at the Metal. *Chem. - Eur. J.* **2008**, *14* (33), 10267–10279. https://doi.org/10.1002/chem.200801373.
(20)Peter K. Byers; Allan J. Canty; Hong Jin; Dennis Kruis; Bertus A. Markies; Jaap Boersma; Gerard Van Koten. Dimethylpalladium(II) and Monomethylpalladium(II) Reagents and Complexes. *Inorg. Synth.* **1998**, *32*, 162–172.
(21)Ben-Tal, Y.; Boaler, P. J.; Dale, H. J. A.; Dooley, R. E.; Fohn, N. A.; Gao, Y.; García-Domínguez, A.; Grant, K. M.; Hall, A. M. R.; Hayes, H. L. D.; Kucharski, M. M.; Wei, R.; Lloyd-Jones, G. C. Mechanistic Analysis by NMR Spectroscopy: A Users Guide. *Prog. Nucl. Magn. Reson. Spectrosc.* **2022**, *129*, 28–106. https://doi.org/10.1016/j.pnmrs.2022.01.001.
(22)Rainer Kerssebaum. *DOSY and Diffusion by NMR*; Rheinstetten, Germany.

6. Supplementary Information

List of Supplementary Figures

Figure S1. ^{1}H NMR of 4-(*tert*-butyl)pyridine-*N*-oxide **55**
Figure S2. ^{1}H NMR of 2-amino-4-(*tert*-butyl)pyridine.....**56**
Figure S3. ^{1}H NMR of 1,3-bis(2-(4-*tert*-butyl)pyridylimino)isoindole **57**
Figure S4. ^{1}H NMR of [(TMEDA)Pd(Cl)$_2$] **58**
Figure S5. ^{1}H NMR of [(TMEDA)Pd(Me)$_2$].....**59**
Figure S6. ^{1}H NMR of [(BPI)Pd(Me)] **60**
Figure S7. ^{1}H NMR of [^{H}(BPI)Pd(Me)][BF$_4$] **61**
Figure S8. ^{19}F{^{1}H} NMR of [^{H}(BPI)Pd(Me)][BF$_4$].....**62**

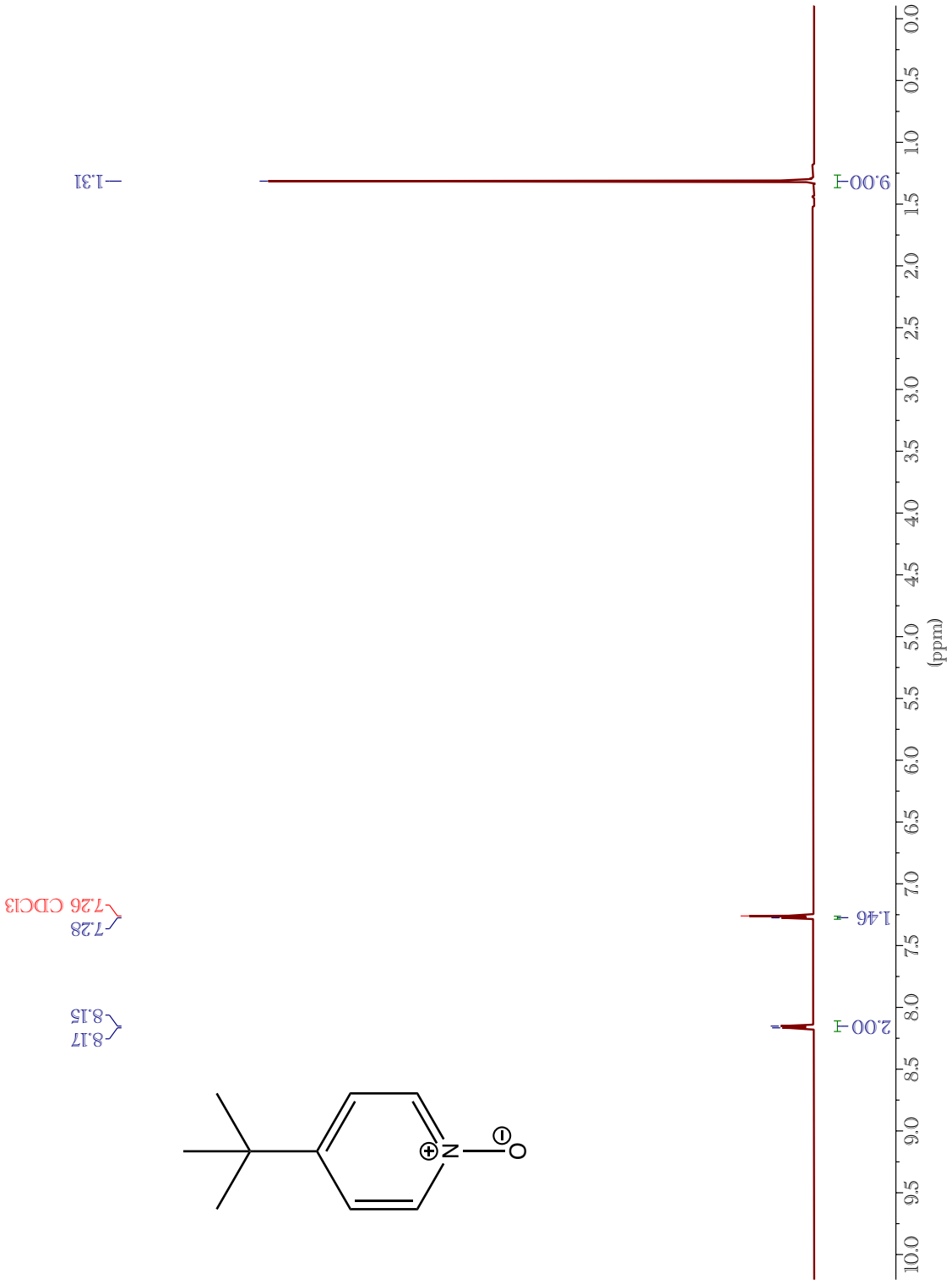

Figure S1. ^{1}H NMR of 4-(*tert*-butyl)pyridine-*N*-oxide (500 MHz; $CDCl_3$; 99% yield): δ 8.16 (d, J = 7.2 Hz, 2H), δ 7.27 (d, 2H), δ 1.31 (s, 9H).

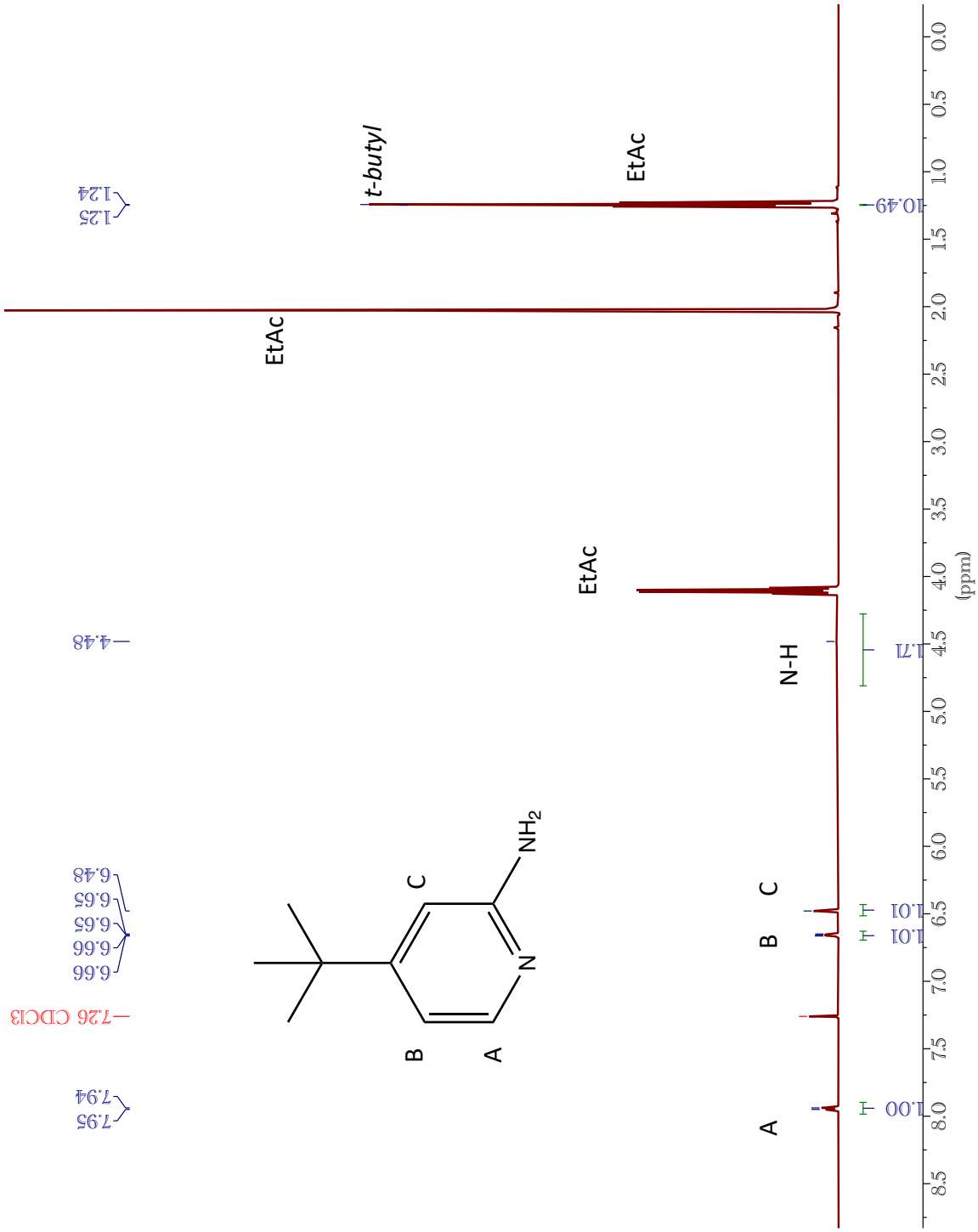

Figure S2. ^{1}H NMR of 2-amino-4-(*tert*-butyl)pyridine (500 MHz; $CDCl_3$; 56% yield): δ 7.94 (d, J = 5.6 Hz, 1H), δ 6.66 (dd, J = 5.5, 1.7 Hz, 1H), δ 6.48 (s, 1H), δ 4.48 (s, 2H), δ 1.25 (d, 9H).

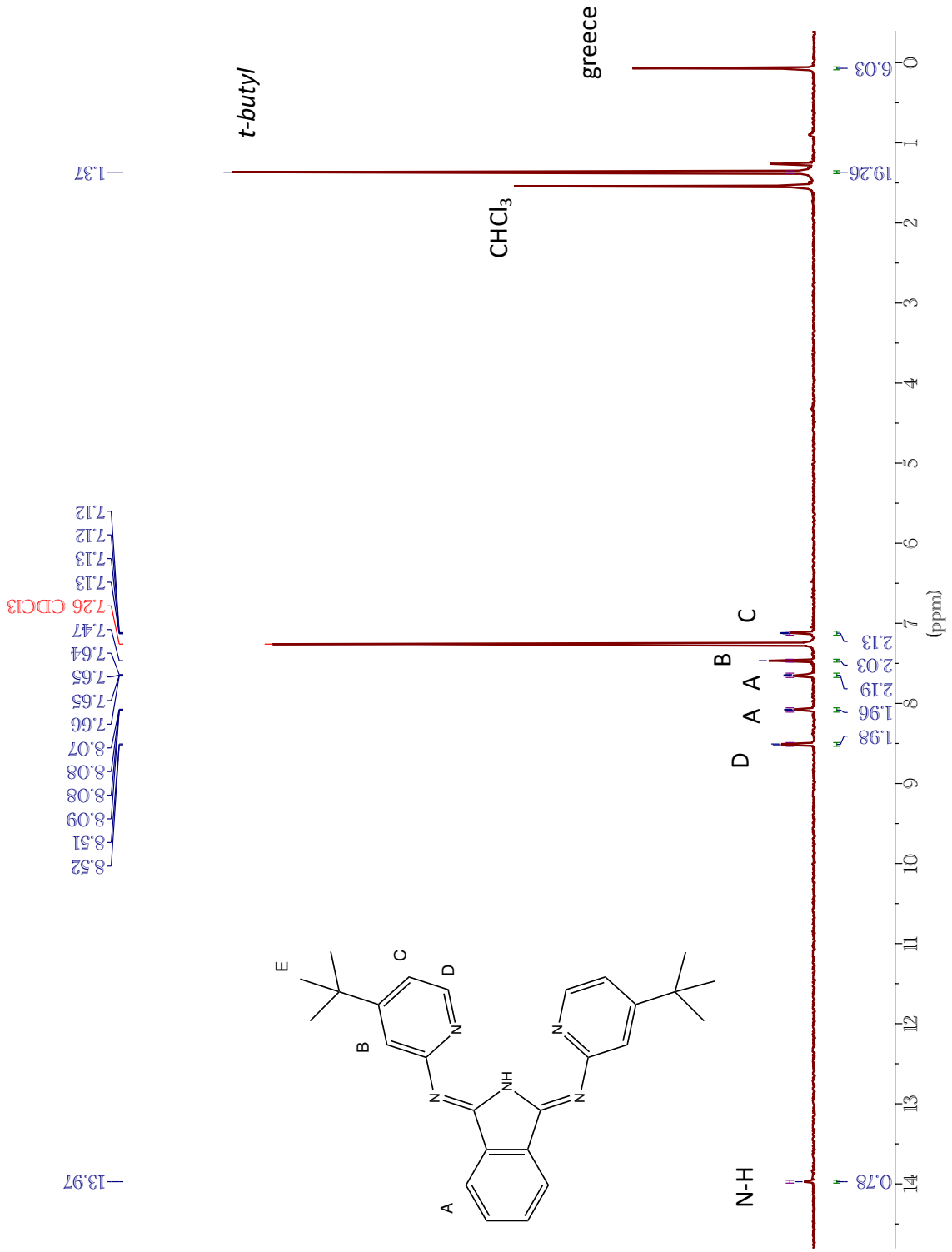

Figure S3. ^{1}H NMR of 1,3-bis(2-(4-*tert*-butyl)pyridylimino)isoindole (500 MHz; $CDCl_3$; 69% yield): δ 13.97 (s, 1H), δ 8.51 (d, J = 5.3 Hz, 2H), δ 8.08 (dd, J = 5.7, 3.1 Hz, 2H), δ 7.65 (dd, J = 5.6, 3.0 Hz, 2H), δ 7.47 (s, 2H), δ 7.12 (dd, J = 5.5, 1.9 Hz, 2H), δ 1.37 (s, 18H).

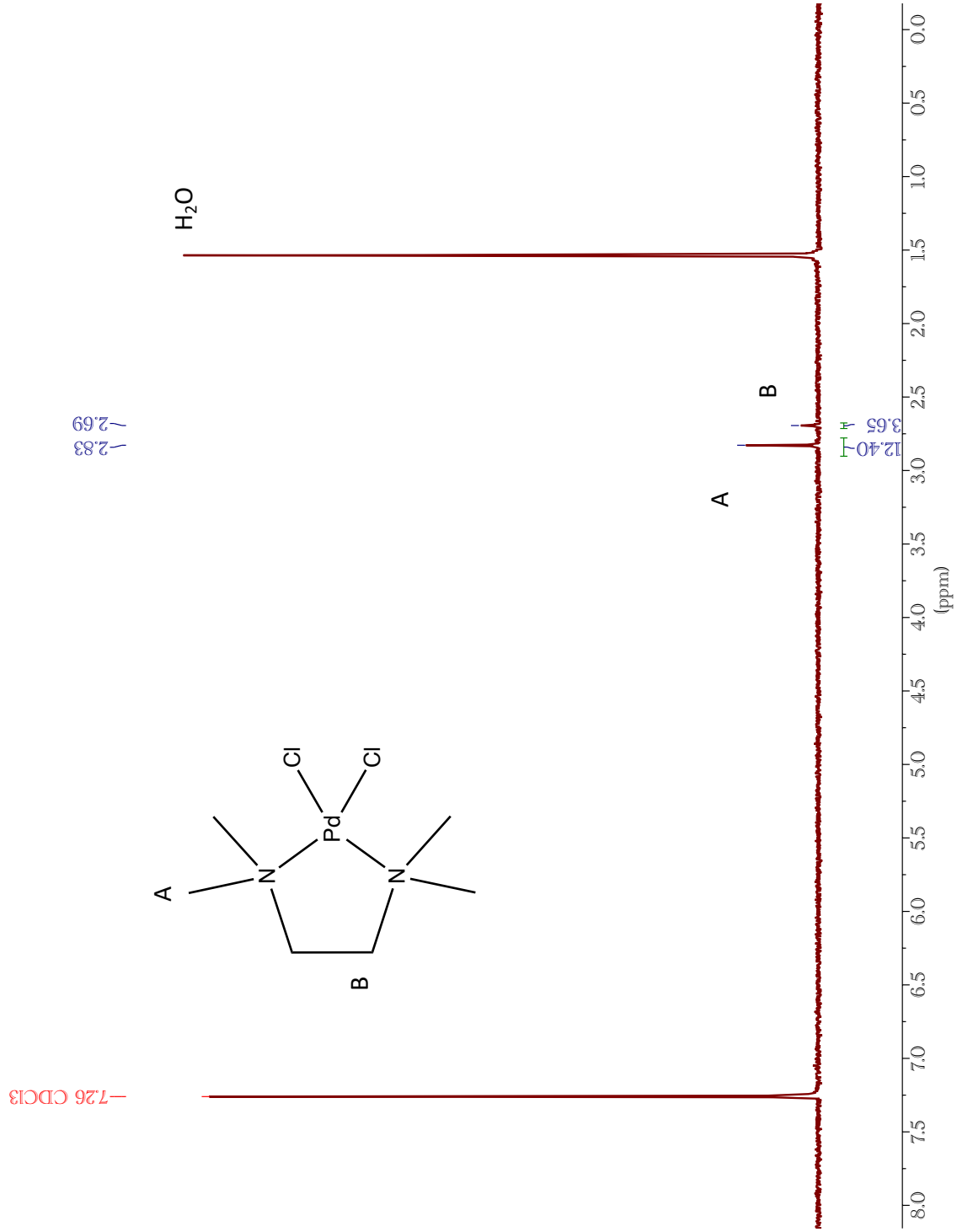

Figure S4. ^{1}H NMR of [(TMEDA)Pd(Cl)$_2$] (500 MHz; $CDCl_3$; 96% yield): δ 2.83 (s, 12H), δ 2.69 (s, 4H).

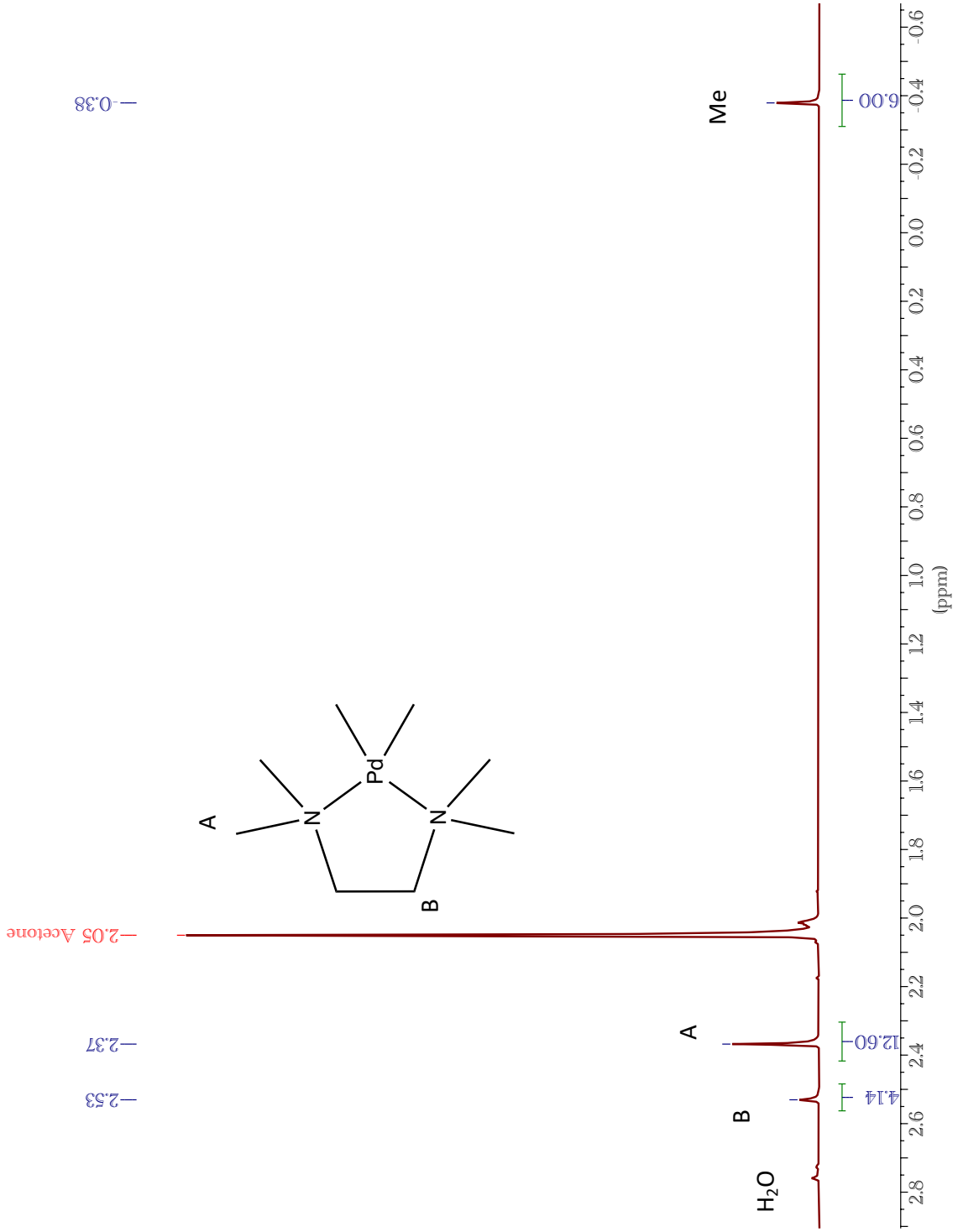

Figure S5. ^{1}H NMR of [(TMEDA)Pd(Me)$_2$] (500 MHz; (CD$_3$)$_2$CO; 52% yield): δ 2.53 (s, 4H), δ 2.37 (s, 12H), δ -0.38 (s, 6H).

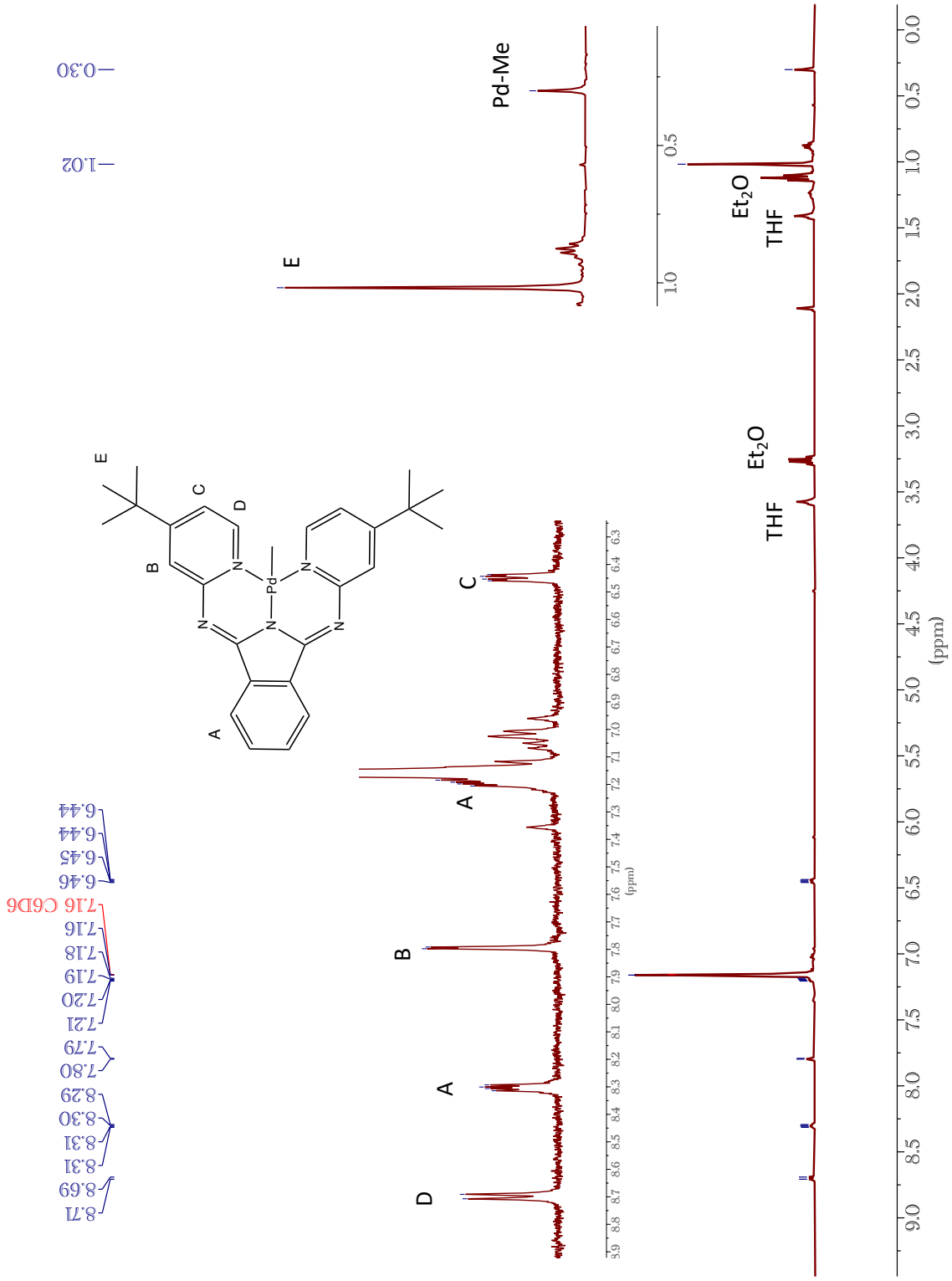

Figure S6. ^{1}H NMR of [(BPI)Pd(Me)] (400 MHz; C_6D_6; 94% yield): δ 8.70 (d, J = 6.6 Hz, 2H), δ 8.30 (dd, J = 5.4, 3.1 Hz, 2H), δ 7.79 (d, J = 2.5 Hz, 2H), δ 7.27 – 7.19 (m, 2H), δ 6.45 (dd, J = 6.5, 2.5 Hz, 2H), δ 1.02 (s, 24H), δ 0.30 (s, 3H).

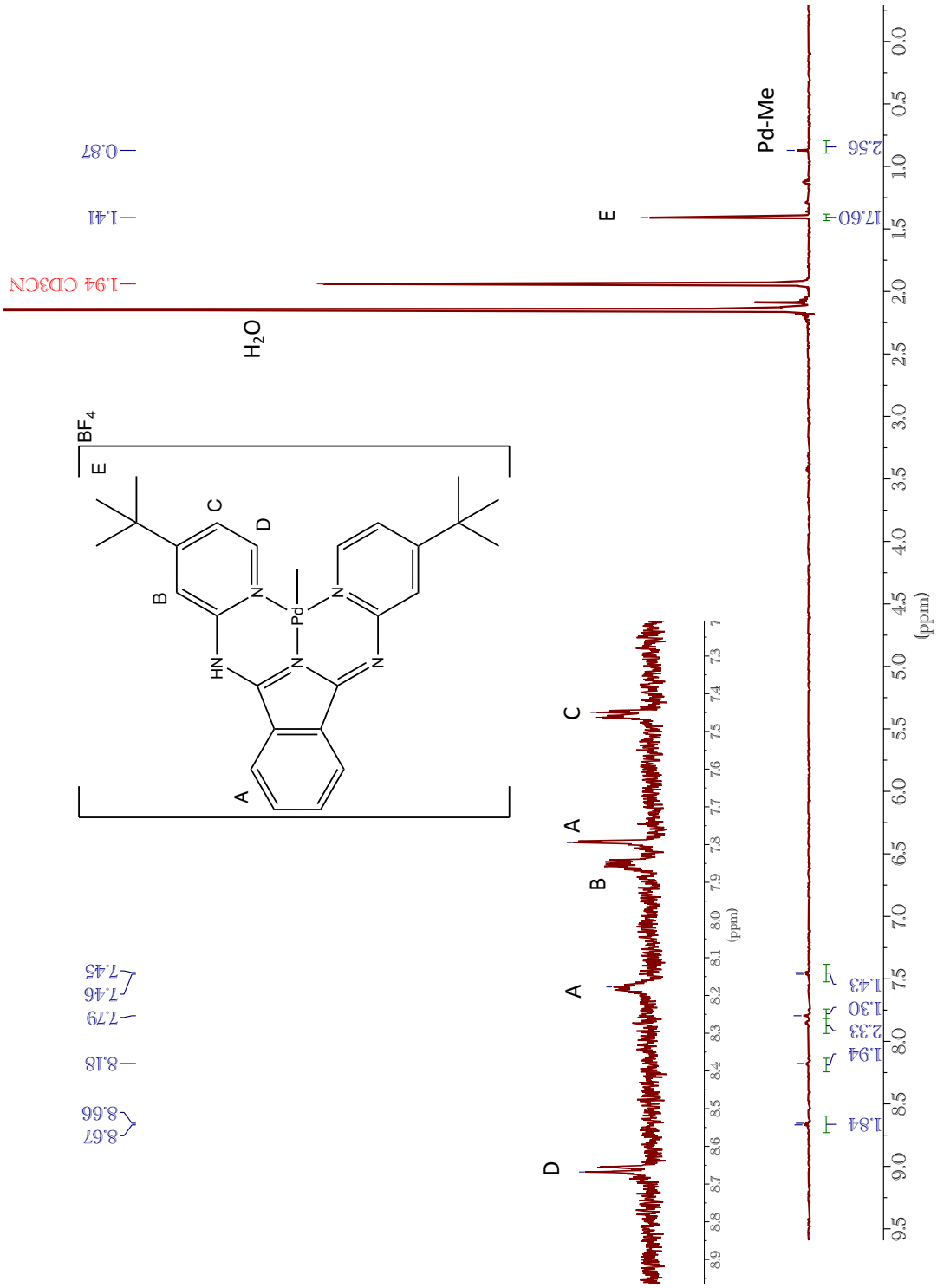

Figure S7. ^{1}H NMR of [^{H}(BPI)Pd(Me)][BF_4] (500 MHz; CD_3CN; 62% yield): δ 8.66 (d, J = 6.4 Hz, 2H), δ 8.18 (s, 2H), δ 7.85 (s, 2H), δ 7.79 (s, 2H), δ 7.46 (d, J = 6.4 Hz, 2H), δ 1.41 (s, 18H), δ 0.87 (s, 3H).

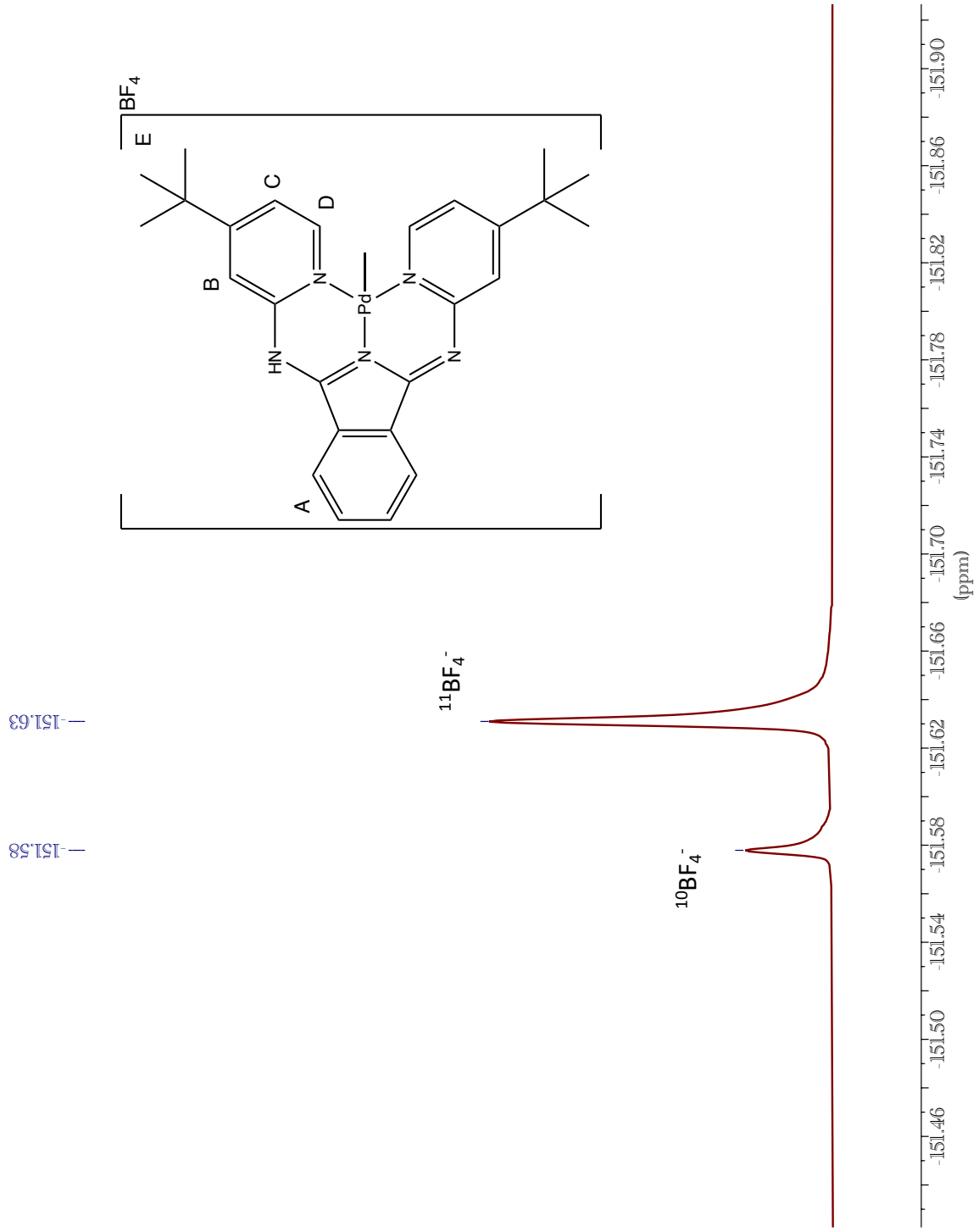

Figure S8. $^{19}F\{^{1}H\}$ NMR of $[^{H}(BPI)Pd(Me)][BF_4]$ (376 MHz; CD_3CN): δ -151.61 (d, 4F).